ARL-TR-8111 ● AUG 2017

US Army Research Laboratory

Modeling, Simulation, and Measurement of Balanced Antipodal Vivaldi (BAV) Antennas for Fully Polarimetric Forward-Looking Ground-Penetrating Radar (FLGPR) Receive Channels

by Seth A McCormick

NOTICES

Disclaimers

The findings in this report are not to be construed as an official Department of the Army position unless so designated by other authorized documents.

Citation of manufacturer's or trade names does not constitute an official endorsement or approval of the use thereof.

Destroy this report when it is no longer needed. Do not return it to the originator.

ARL-TR-8111 ● AUG 2017

US Army Research Laboratory

Modeling, Simulation, and Measurement of Balanced Antipodal Vivaldi (BAV) Antennas for Fully Polarimetric Forward-Looking Ground-Penetrating Radar (FLGPR) Receive Channels

by Seth A McCormick
Sensors and Electron Devices Directorate, ARL

REPORT DOCUMENTATION PAGE

Form Approved
OMB No. 0704-0188

1. REPORT DATE *(DD-MM-YYYY)*	2. REPORT TYPE	3. DATES COVERED (From - To)
August 2017	Technical Report	May 2016–January 2017

4. TITLE AND SUBTITLE
Modeling, Simulation, and Measurement of Balanced Antipodal Vivaldi (BAV) Antennas for Fully Polarimetric Forward-Looking Ground-Penetrating Radar (FLGPR) Receive Channels

5a. CONTRACT NUMBER

5b. GRANT NUMBER

5c. PROGRAM ELEMENT NUMBER

6. AUTHOR(S)
Seth A McCormick

5d. PROJECT NUMBER

5e. TASK NUMBER

5f. WORK UNIT NUMBER

7. PERFORMING ORGANIZATION NAME(S) AND ADDRESS(ES)
US Army Research Laboratory
Sensors and Electron Devices Directorate
ATTN: RDRL-SER-M
2800 Powder Mill Road, Adelphi, MD 20783-1138

8. PERFORMING ORGANIZATION REPORT NUMBER
ARL-TR-8111

9. SPONSORING/MONITORING AGENCY NAME(S) AND ADDRESS(ES)

10. SPONSOR/MONITOR'S ACRONYM(S)

11. SPONSOR/MONITOR'S REPORT NUMBER(S)

12. DISTRIBUTION/AVAILABILITY STATEMENT
Approved for public release; distribution is unlimited.

13. SUPPLEMENTARY NOTES

14. ABSTRACT
This report documents the design, simulation, and measurement of balanced antipodal Vivaldi (BAV) antenna elements for the receive channels of a US Army Research Laboratory fully polarimetric forward-looking ground-penetrating radar (FLGPR) system including recommendations for the antenna positioning in a 32-element aperture. The BAV elements are meant to be operated from 0.3 to 2.0 GHz in a stepped frequency system. The elements are designed to have improved antenna performance compared to the current receive channel antennas below 1.0 GHz. The BAV elements have significantly improved realized gain and impedance match over the operational bandwidth. The elements also have an improved transient response with reduced late time ringing. Pairs of elements were simulated in different side-by-side configurations to determine effects on individual antenna performance and mutual coupling. Simulations showed that the configuration to produce the most compact 32-element aperture at 2.2 m wide was that of vertical and horizontal elements positioned such that they produce an "L" shape. However, isolation between vertical and horizontal elements was considered critical, so a "T"-shaped configuration instead of an L shape would be preferred. Such an aperture would be nearly twice as wide at 4 m.

15. SUBJECT TERMS
balanced antipodal Vivaldi, tapered slot, FLGPR, antenna design and simulation, UWB antennas

16. SECURITY CLASSIFICATION OF:			17. LIMITATION OF ABSTRACT	18. NUMBER OF PAGES	19a. NAME OF RESPONSIBLE PERSON
a. REPORT	b. ABSTRACT	c. THIS PAGE			Seth A McCormick
Unclassified	Unclassified	Unclassified	UU	64	19b. TELEPHONE NUMBER (Include area code) (301) 394-2706

Contents

List of Figures

Acknowledgments

I would like to acknowledge Arthur C Harrison for assembling the balanced antipodal Vivaldi antennas and the foam support structure. I would also like to acknowledge William O Coburn for his technical advice in the analysis of the balanced antipodal Vivaldi.

1. Introduction

This report documents the design by simulation of a pair of balanced antipodal Vivaldis (BAVs) for the receive channels of an ultra-wideband (UWB) fully polarimetric forward-looking ground-penetrating radar (FLGPR). A particular challenge when designing a UWB antenna for FLGPR is meeting performance requirements in a practical size (i.e., can still be mounted on a commercial vehicle and fit within the width of a typical highway lane). Low-frequency performance drives antenna size. Operating at lower frequencies improves ground penetration and would allow the FLGPR operator to see objects buried deeper within the ground as predicted by the skin depth of a lossy half space.[1] However, the direct relationship between antenna size (performance) and wavelength requires that the antenna must be electrically larger to improve the low-frequency performance.[2] Often this requires antennas that are large physically, and in the case of material loading, produce antennas that are smaller physically with the same electrical size but with reduced performance. The metrics by which the antenna performance is gauged are efficiency (i.e., realized gain) and the impedance match (i.e., reflection coefficient). In addition, both cross polarization (cross-pol) isolation between cross-pol receive antennas, which provides a metric for antenna positioning, and characterizing the voltage transient of the antenna for a given input pulse (low late time ringing) are of concern. Other metrics such as the front-to-back ratio (F/B) and half-power beamwidth are also included.

The next section discusses the design requirements for the receive antennas and overviews the current receiver to be improved upon. Section 3 shows the measured and simulated results for the current Vivaldi and discusses the 3 antennas considered as replacements. Section 4 discusses the BAV and the design by simulation. Section 5 shows the evaluation of the BAV performance by comparison of the measured and simulated results. Section 6 discusses the positioning of paired cross-pol BAVs and the impact on performance and isolation, and Section 7 summarizes and concludes the report with final statements.

2. Problem Statement

The FLGPR system is an in-house-developed system. It is fully polarimetric and currently uses 16 Vivaldi antennas for the 16 receive channels, one of which is shown in Fig. 1. The transmit channels are switched and use 2 dual-pol ridged horns with one on either side of the receive aperture. The Vivaldi has dimensions 4.9 × 16.8 × 0.3 inches^3 (length × width × thickness) with a weight of 2.23 lb. It was milled on stacked Rogers Duroid 5880 substrate ($\varepsilon_r = 2.2$ and $\tan\delta_e = 0.001$). The

top and bottom sides are identical. The Vivaldi is fed using a tapered stripline ending in a sectoral flare that is centered between the top and bottom surfaces. Brass shimming was soldered on the outside for improved structural integrity.

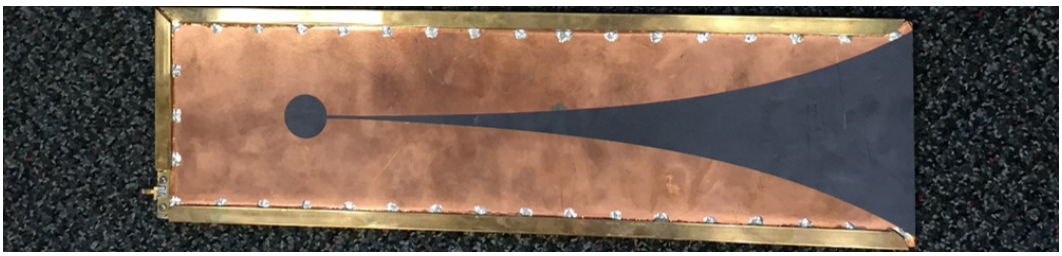

Fig. 1 Current Vivaldi receive antenna for US Army Research Laboratory FLGPR

The Vivaldi was operated over the frequency range of 0.3–2.0 GHz for both vertical and horizontal receive channels. The horizontal spacing between elements is about 5 inches center-to-center. Dual-pol operation is achieved by mechanically rotating the elements in between measurements. The small size of the Vivaldi limits the low-frequency performance (<1.0 GHz) in terms of the impedance match and the realized gain, but just increasing the Vivaldi size alone is not enough. A complete new design is necessary as the stripline must also be redesigned and the transient response is not particularly smooth with large late-time ringing. Additionally, mechanically rotating the elements is impractical for mobile system performance (i.e., introduced mechanical delay). The goal of the design process is to improve the low-frequency performance while achieving dual-pol operation without mechanical means. Additional requirements are to maximize cross-pol isolation (i.e., isolation between cross-pol elements) and to maintain a small enough form factor to fit 32 elements within a width of 2.2 m; as will be shown, these 2 requirements are in opposition to each other.

3. Current Vivaldi Elements and Replacement Antennas Considered

The majority of the design process was conducted through modeling and simulation, including comparisons between the designed antennas and the Vivaldi to be replaced. The commercial computational electromagnetic software FEKO and General Electromagnetic Solver (GEMS) were used for modeling and simulation.[3,4] FEKO was the primary computer-aided design (CAD) tool with simulation results using the Method of Moments (MoM) to produce the interaction matrix and Lower-Upper decomposition for solving the MoM matrix. GEMS was the primary simulation tool, as the Finite Difference Time Domain solver was well suited for efficiently simulating UWB antennas. FEKO was used as a check for code-to-code comparisons. A model for the Vivaldi was built in FEKO from published drawings

and is show in Fig. 2.[5] Neither the connector nor the notch around the connector was included in the model. The sides of the Vivaldi are metallic; the metal is modeled using infinitesimally thin perfectly electrically conducting (PEC) surfaces.

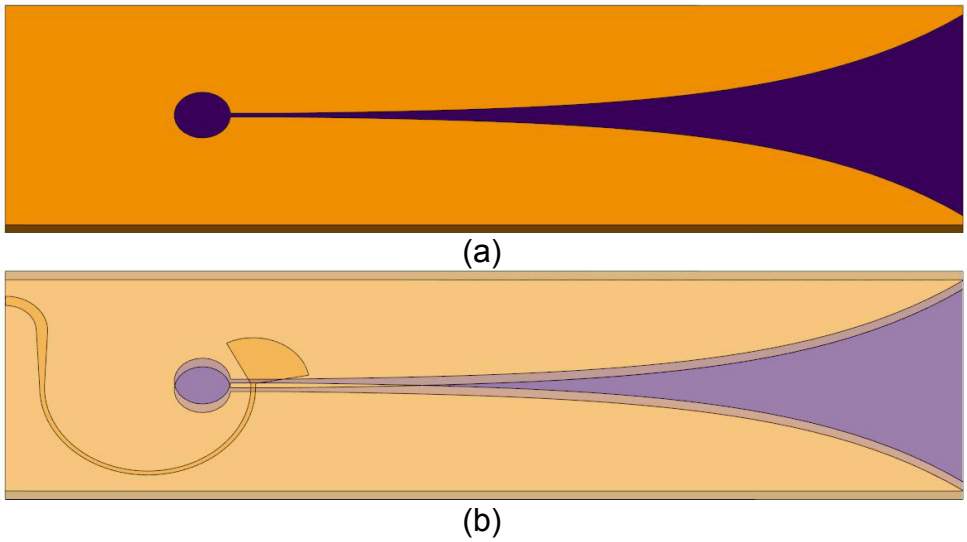

Fig. 2 FEKO Vivaldi model a) top view and b) partially transparent view

The simulated and measured comparisons of the Vivaldi reflection coefficient and realized gain are shown in Figs. 3a and 3b, respectively. The excitation is a simple wire port in both FEKO and GEMS. The input pulse in the time domain is a differentiated Gaussian pulse with a high frequency of 4 GHz. The FEKO results are only calculated up to 1.2 GHz because of computational memory limitations and time to solution. It is understood that the model comparisons may start to break down at higher frequencies because of the mesh. The code-to-code agreement is good, but the comparison with measured data is not as good as expected for the reflection coefficient. Not including the connector and cutout would be the most likely reasons, but increasing the model complexity was not necessary. Material losses could also be a reason for the reduction in oscillations (reduced resistance) in the impedance as shown by the reflection coefficient, Fig. 3a. The Vivaldi impedance may also be sensitive to the metal thickness as it is virtually a slot-type antenna under the class of tapered slot antennas. Slot antennas are known to be sensitive to the thickness of the metal from which they are constructed, even if the metal is thin. The dependency on the slot thickness will become more important as the simulation frequency increases. The trend in the simulated reflection coefficient and realized gain is similar enough to the measured data to be used as an appropriate baseline for model-to-model comparisons. Absolute accuracy was not a concern for the model validation in this case for comparing alternative prototypes.

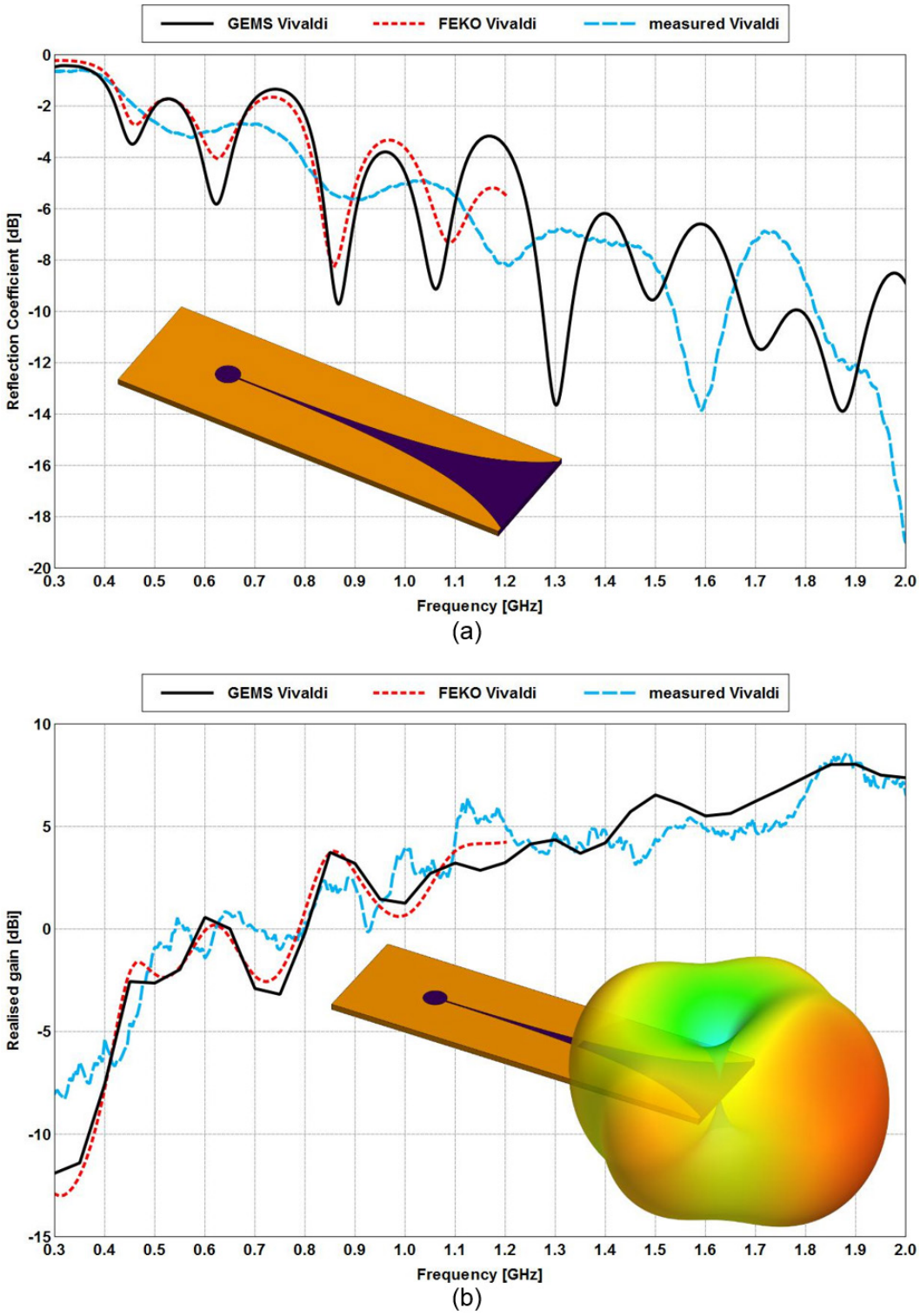

Fig. 3 Simulated and measured comparison of Vivaldi a) reflection coefficient and b) realized gain vs. frequency

The antennas considered as alternatives are shown in Figs. 4a–c. The antipodal planar logarithmic periodic dipole array (LPDA) antenna element, Fig. 4a, had been designed for a previous forward-looking system.[6] The LPDA is UWB with reasonably stable high gain as shown in the FEKO results, Figs 5a and 5b. This particular LPDA is also more compact than typical. As with all LPDAs, it must be fed with a coax that is only soldered to the antenna at the end with the short elements. While this antenna has desirable gain, the bandwidth that could be achieved would fall short of the requirement, and unlike other types of antennas where the low-frequency impedance match may gracefully worsen, the LPDA impedance match rapidly decays, as can be seen in the reflection coefficient, Fig. 5a. Given the size limitations and the fact that the antennas are to function over the transmit bandwidth, it is preferred to have an antenna that matches the former impedance behavior.

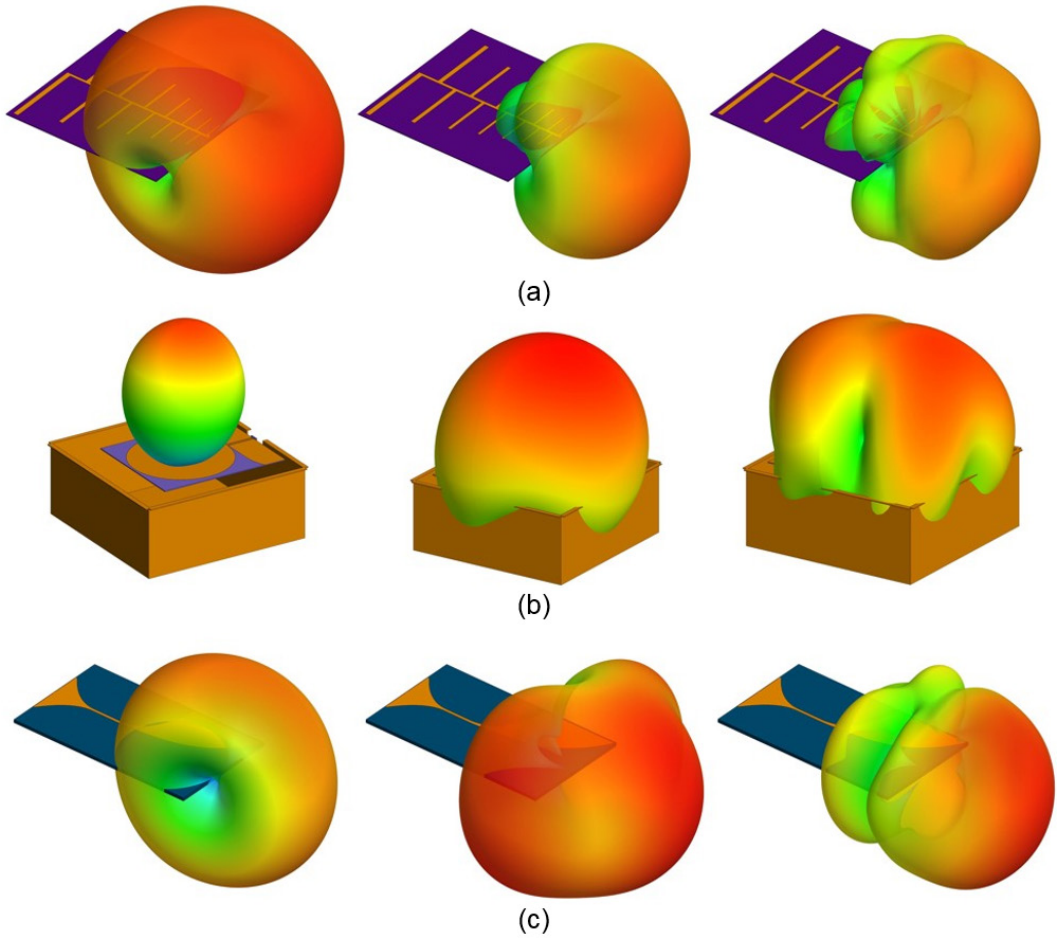

Fig. 4 Candidate antenna elements for ARL FLGPR: a) antipodal planar LPDA, b) cavity-backed UWB planar circular monopole, and c) balanced antipodal Vivaldi. The radiation patterns are at 0.3, 0.6, and 1.2 GHz on a 60-dB scale.

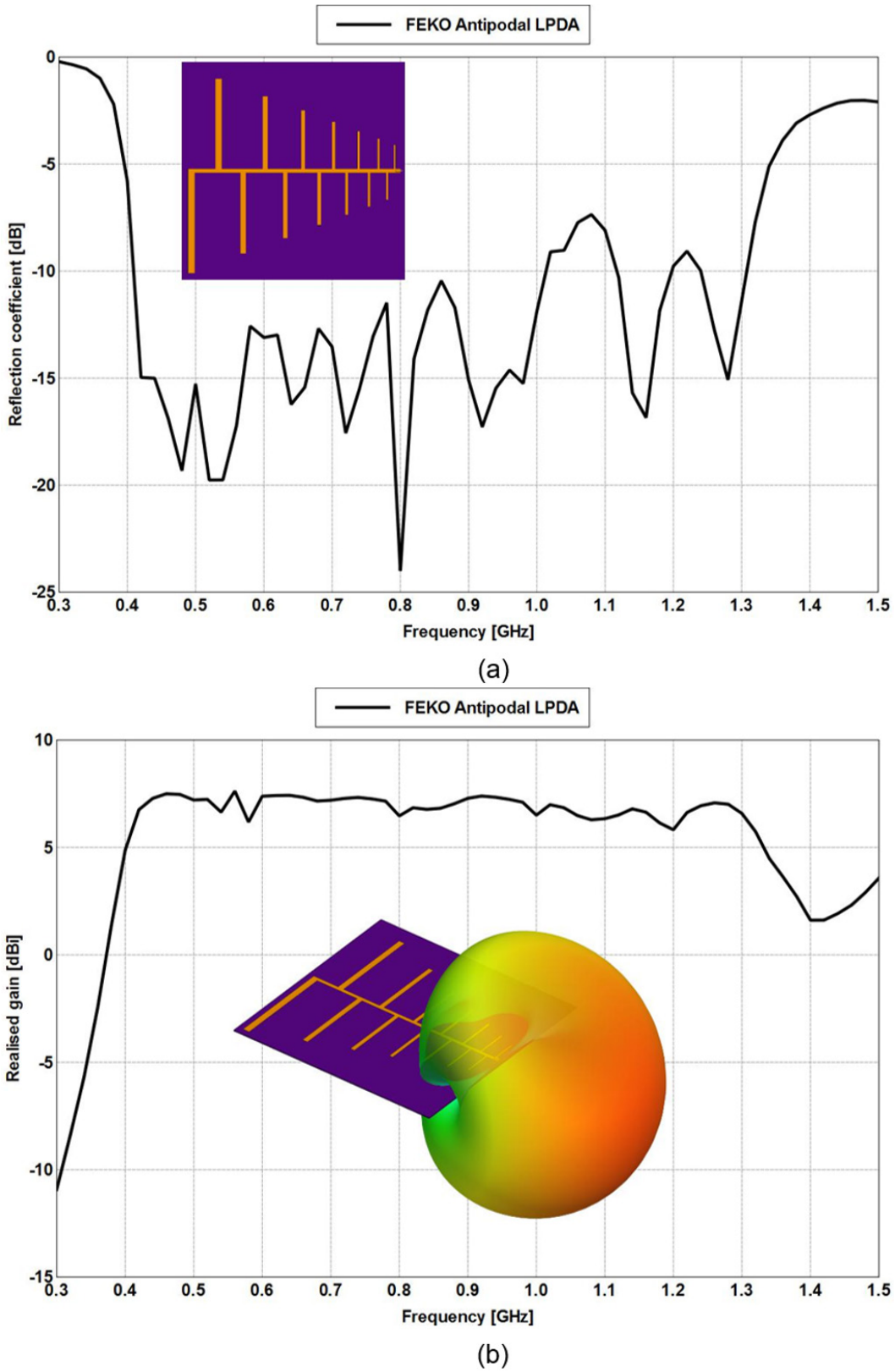

Fig. 5 Planar LPDA-simulated a) reflection coefficient and b) realized gain vs. frequency

Figure 4b shows a cavity-backed UWB planar circular monopole that had been designed for a FLGPR system that operated from 0.3 to 1.2 GHz.[7] This antenna is advantageous in that its forward dimension is much smaller than that of the Vivaldi (i.e., reduced depth), although it requires a cavity backing to produce unidirectional radiation. The monopole alone is matched over the near decade bandwidth, but like all other planar monopoles, it has an increasing pattern tilt away from the feed, with frequency, toward end-fire; this is a consequence of a traveling wave behavior that occurs as the monopole becomes electrically longer. The pattern tilt occurs within the second octave. At frequencies greater than the second octave, the beam peak splits and tilts further, producing a null on boresight and lower gain at broadside. Modifications can be made to help reduce the severity of the pattern tilt and increase realized gain, but such modifications typically produce positive results up to the end of the second octave. The cavity-backed monopole is a significant improvement over the Vivaldi, as seen in the voltage standing wave ratio (VSWR), Fig. 6a, and realized gain, Fig. 6b, but cannot operate up to 2 GHz because of the pattern instability.

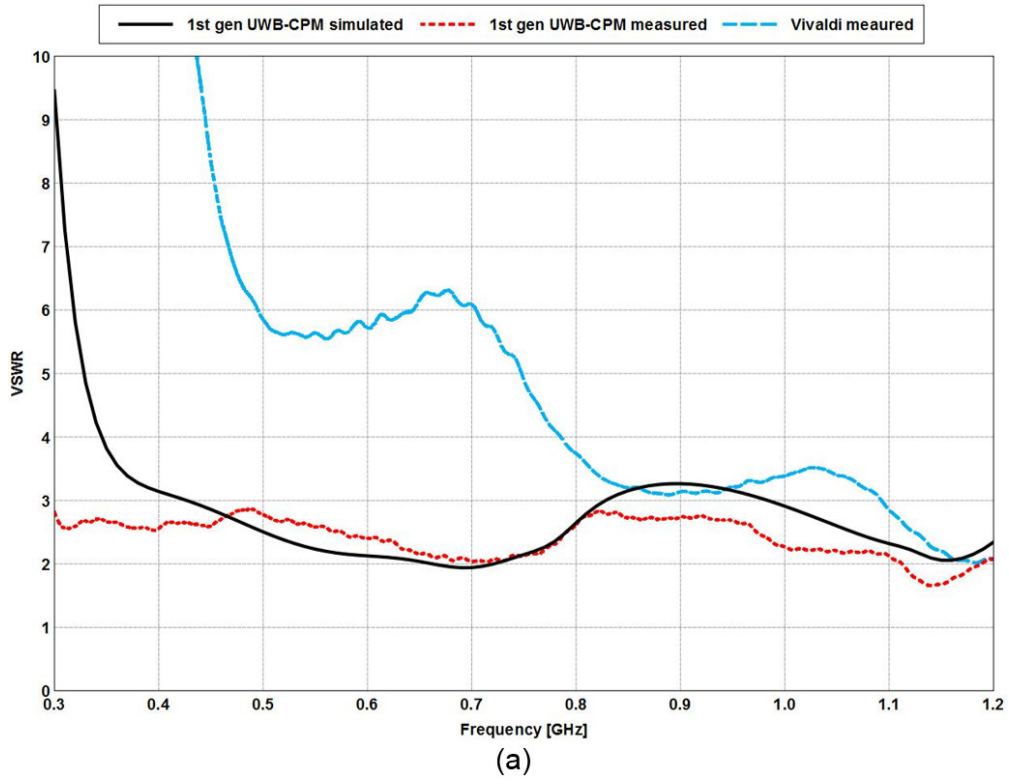

Fig. 6 Cavity-backed UWB planar circular monopole a) VSWR and b) realized gain vs. frequency compared to the current Vivaldi. Beam peak position is given by the theta angle from broadside.

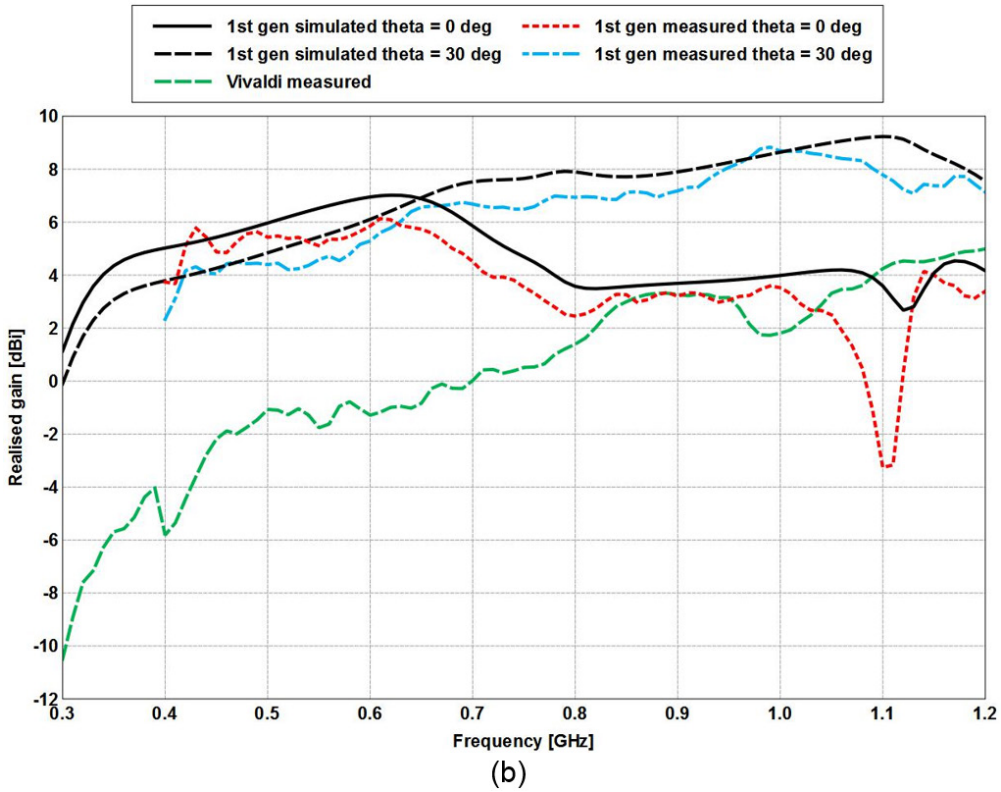

Fig. 6 Cavity-backed UWB planar circular monopole a) VSWR and b) realized gain vs. frequency compared to the current Vivaldi. Beam peak position is given by the theta angle from broadside (continued).

Where the LPDA fails to meet the bandwidth requirement and the cavity-backed UWB planar circular monopole fails to meet the operational bandwidth due to pattern instability, the BAV can supersede on both fronts. The BAV has both a more gracefully deteriorating impedance match than the LPDA and a more stable radiation pattern than the monopole without requiring a backing to achieve unidirectional (or near so) radiation. Another advantage of the BAV versus a traditional tapered slot is that it does not need a quarter wave fanned stub terminated strip to achieve broadband performance, but instead, the BAV is fed with a tapered stripline—a broader band and more simple solution as it does not require a quarter wave stub.

4. BAV Design by Simulation

Figure 7 shows the final built BAV and CAD model. It has dimensions of 10 × 17.2 × 0.25 inches^3, which is similar in length and thickness to the Vivaldi but about twice as wide. The BAV is a stacked structure with 2 substrates that in total has 3 metal layers. The outer fins are mirror copies of each other and are connected to ground. The inner fin flares toward the opposite direction of the outer fins and has

a thin strip to connect to the SubMiniature version A center pin. It was milled in house from two 150-mil Rogers Duroid 5880 substrates with 0.5-oz copper cladding. The antenna was milled in 4 pieces, which were overlapped and attached using double-sided 3M adhesive and 22 nylon screws and nuts. A solder connection electrically joins the two halves for each of the 3 striplines (i.e., top, bottom, and middle). A notch 0.4 inch wide and 0.3 inch deep was cut into the top layer to reveal the pin so that it could be soldered to the center stripline after the BAV was assembled. A piece of brash shimming was then cut and soldered overtop of the notch to cover the center pin and provide a ground contact for the outer fin. Simulations showed that the effect of asymmetry at the feed caused by 2 different dielectric regions (one air and one Duroid) on opposite sides of the stripline is minimal.

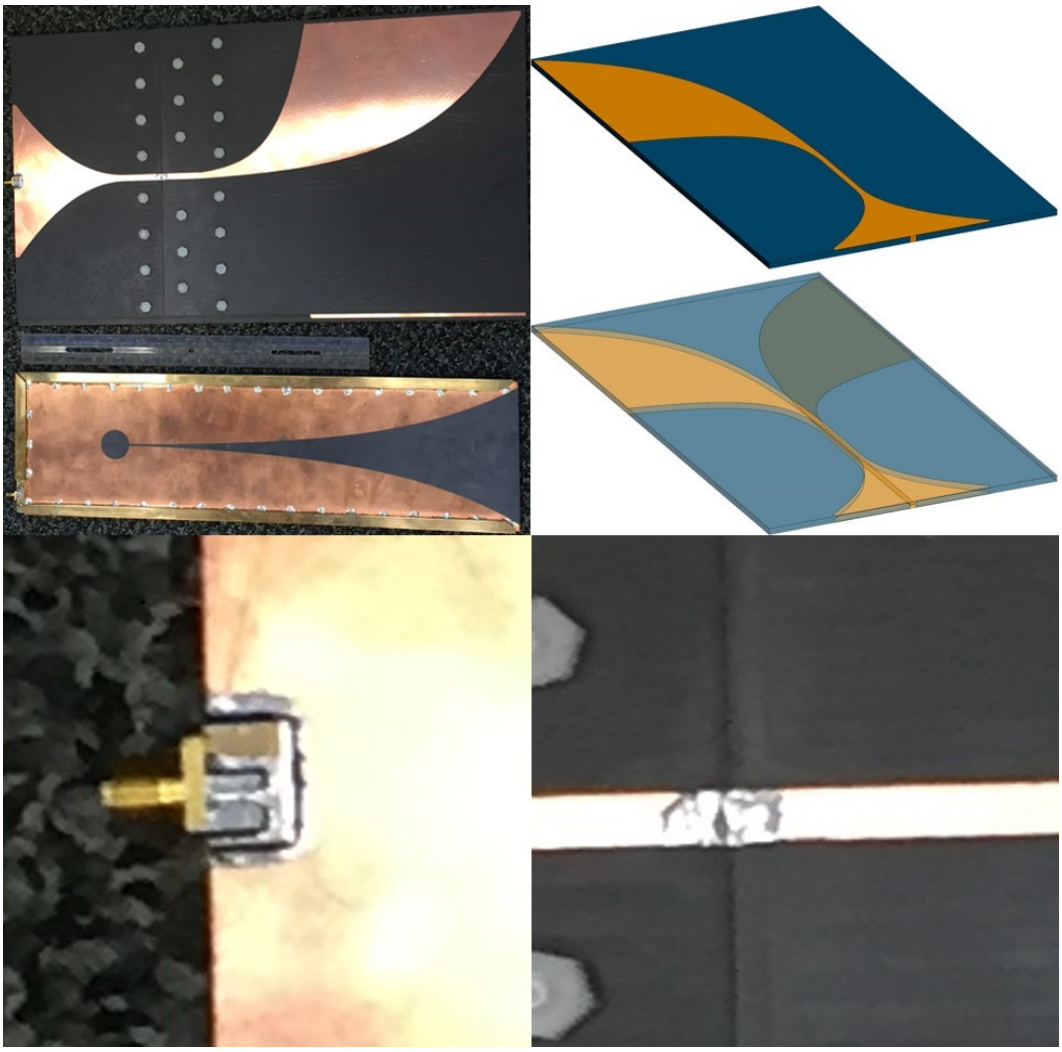

Fig. 7 Built BAV, FEKO model, and Vivaldi (top), and the connector and one of the 3 solder connections (bottom)

The BAV is based off of a design found in the literature.[8] The source paper focused on reducing the length of the BAV to make it more compact at the cost of high-frequency performance. The advantage of the BAV versus other tapered slot antennas is that it has broader bandwidth, owed to the stripline feed, and improved cross-pol rejection.[9,10] The larger cross-pol rejection is caused by the mirrored ground fins cancelling the cross-polarized electric field component through superposition of opposing vectors.[10] Figure 8 shows the original BAV with reduced depth. The shorter flare length reduces the high-frequency gain but improves the low-frequency response and gain by introducing a dipole resonance with its half-wavelength dipole length being the width of the flat edge of the flare. Some of the parameters for the BAV were missing in the reference and had to be estimated from images provided. After having reproduced the reflection coefficient found in Guillanton et al.[8], the reduced-profile BAV dimensions were increased by a factor of $\frac{10}{3}$ to shift the reflection coefficient to lower frequencies.

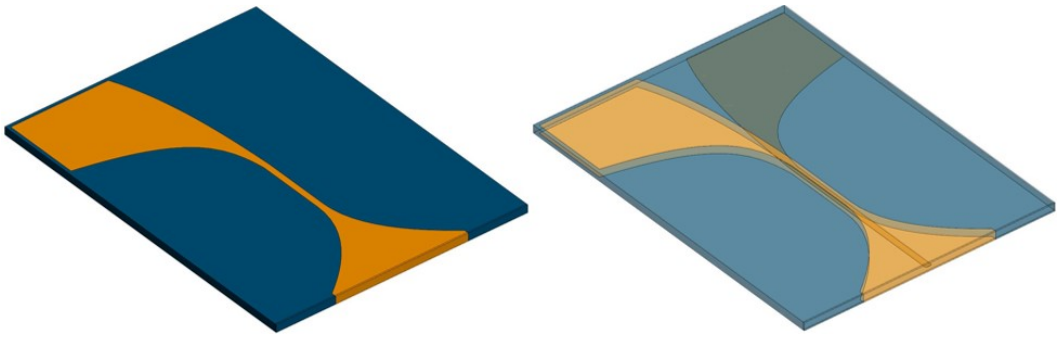

Fig. 8 Original BAV from the literature with reduced depth

Figure 9a shows the simulated reflection coefficient for the reduced-profile BAV after scaling using GEMS and FEKO. The simulated results show that the antenna does not quite meet the standard –10-dB reflection coefficient definition for bandwidth, but this reflection coefficient translates to a VSWR less than 2.5, which is acceptable. The realized gain, Fig. 9b, shows up to 4 dB more gain below 0.7 GHz than the Vivaldi, comparable gain between 0.7 and 1.7 GHz, and at least 2 dB less gain than the Vivaldi above 1.7 GHz. While the reduced-profile BAV is shorter in length than the Vivaldi by 6–7 inches, the lower gain above 1.7 GHz caused by the shorter flare was not acceptable. Simulations comparing reflection coefficient and realized gain for the reduced-profile BAV with percentage increases in flare length and percentage increases in both flare length and flare width were performed in GEMS to determine the combination that achieved the overall best impedance match and realized gain.

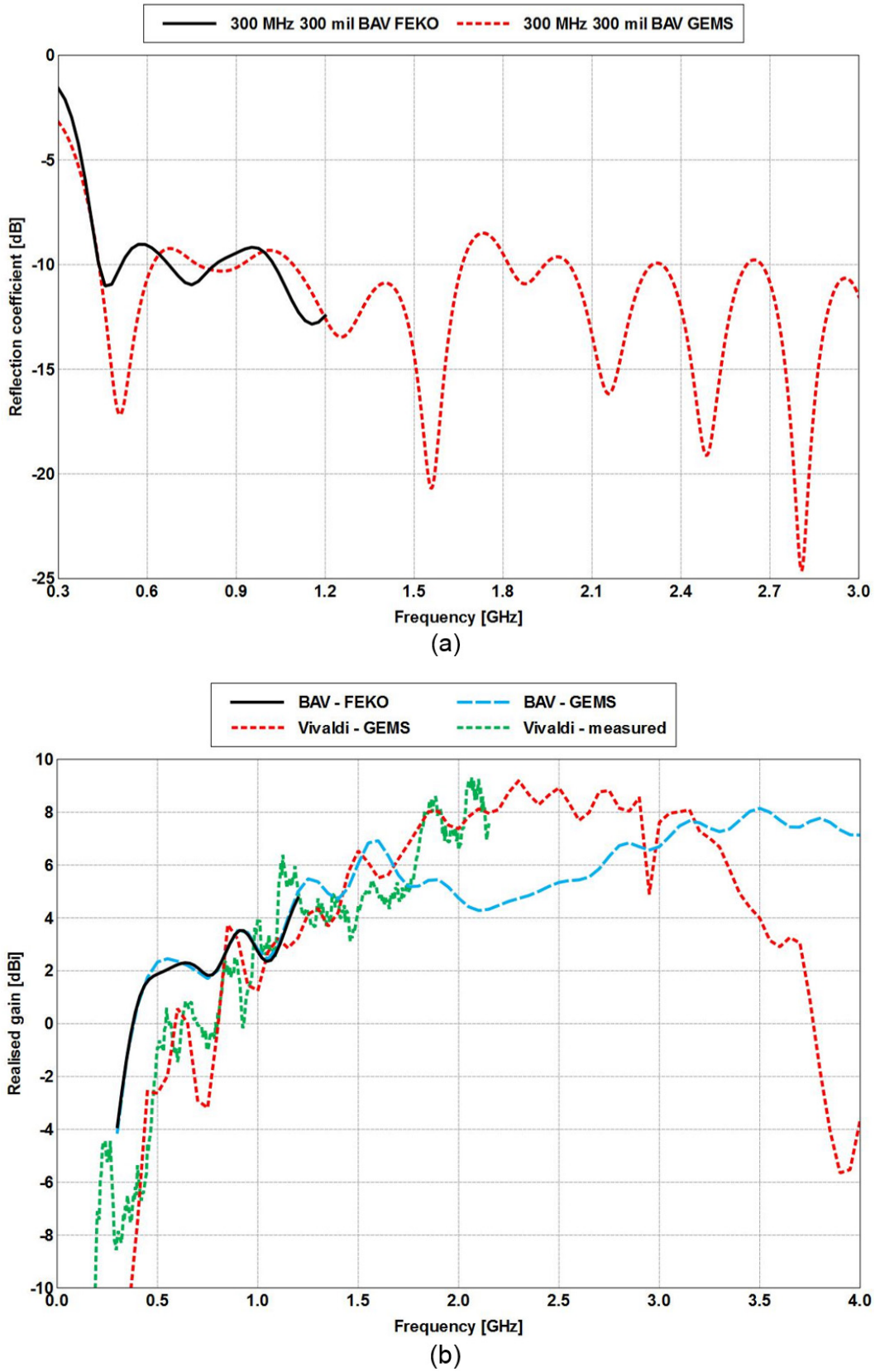

Fig. 9 Reduced depth BAV a) reflection coefficient and b) realized gain vs. frequency

Figures 10a and 10b show the simulated reflection coefficient and realized gain versus frequency for percentage increases in flare length while maintaining the same exponential taper (i.e., start and end opening widths do not change). Increasing the flare length shifts the low-frequency match at 0.5 GHz closer to 0.35 GHz and improves the impedance match above 0.6 GHz. The increased length also improves the realized gain above 0.6 GHz but reduces the gain below 0.6 GHz and produces minimal improvement in the gain above 1.7 GHz. Figures 11a and 11b show the same simulations but with the taper end width increased by the same percentage as the flare length. Again, the low-frequency match is shifted to near 0.3 GHz and the match is improved above 0.6 GHz. Unlike the increase in flare length–only simulations, the gain is improved by 2–3 dB above 1.7 GHz while giving up some gain below 0.7 GHz. The flare length and taper width increase of 60% was chosen as it has the best impedance match and gain over the frequency band.

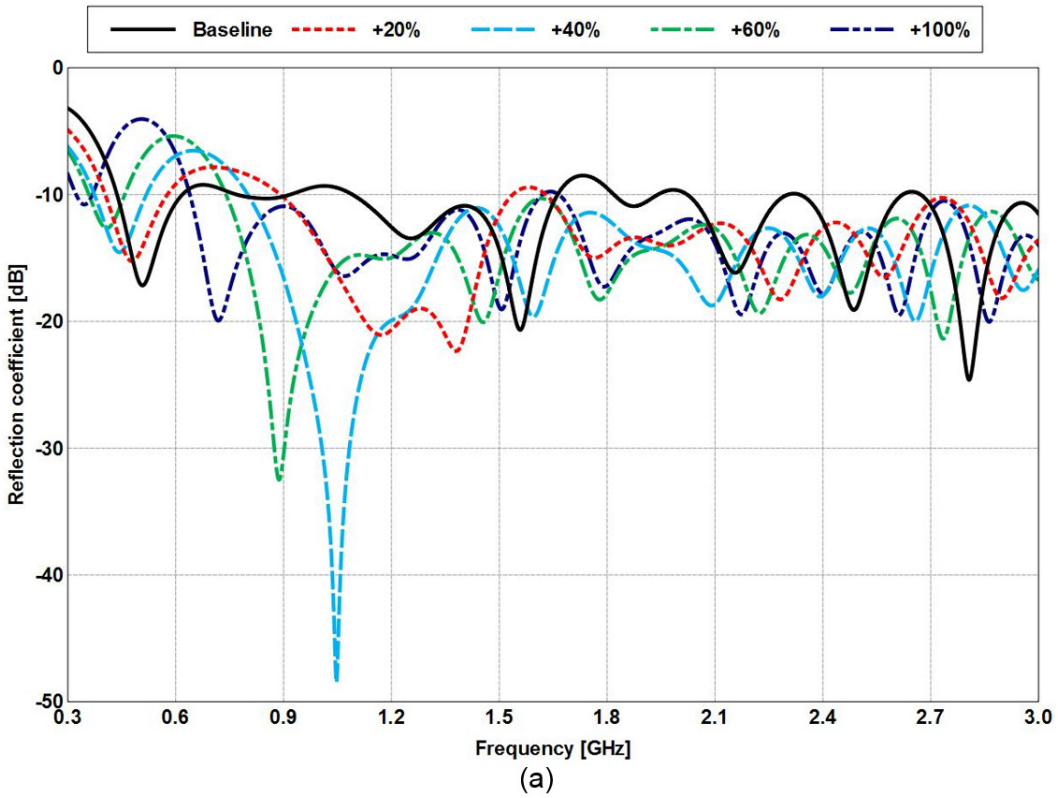

Fig. 10 Simulated a) reflection coefficient and b) realized gain vs. frequency for percentage increases in flare length without changing taper

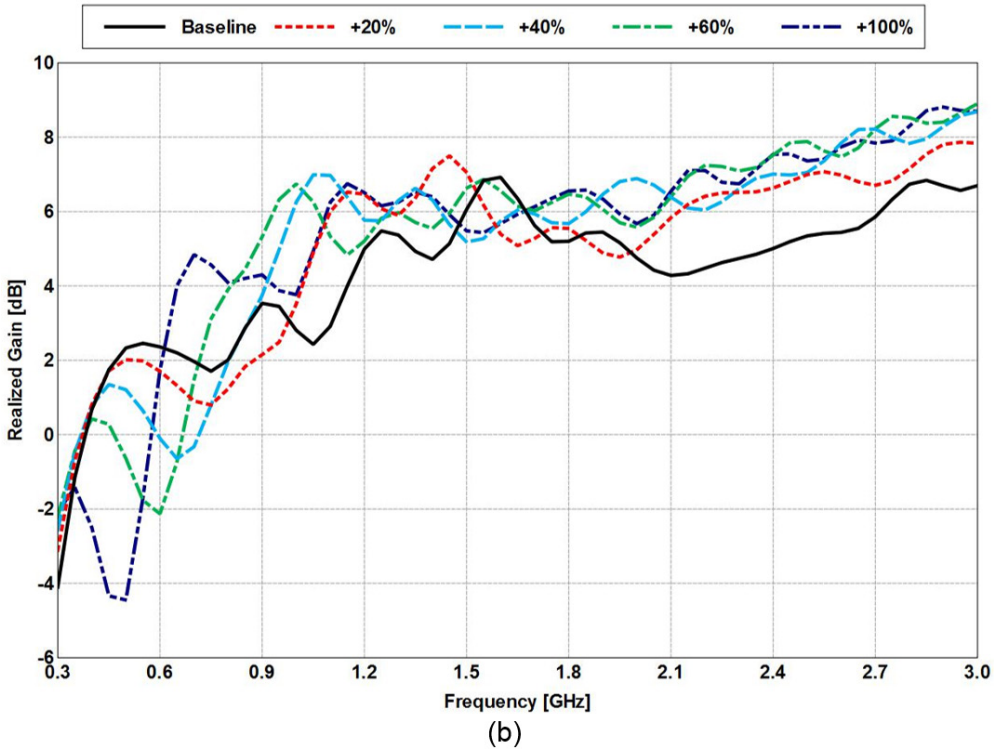

Fig. 10 Simulated a) reflection coefficient and b) realized gain vs. frequency for percentage increases in flare length without changing taper (continued)

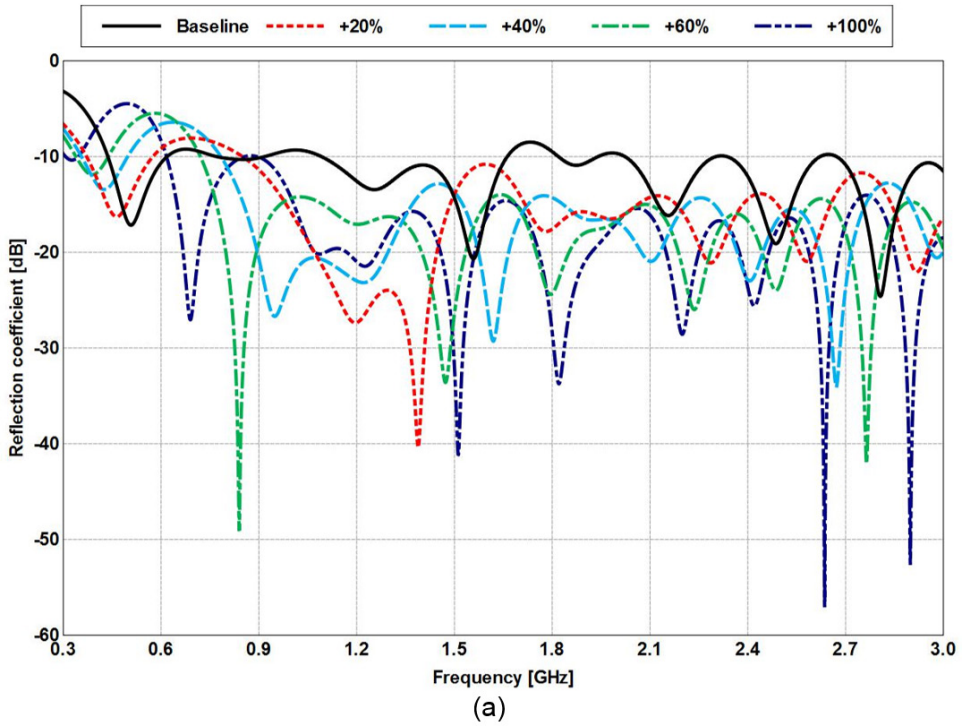

Fig. 11 Simulated a) reflection coefficient and b) realized gain vs. frequency for percentage increase in flare length and ending taper width

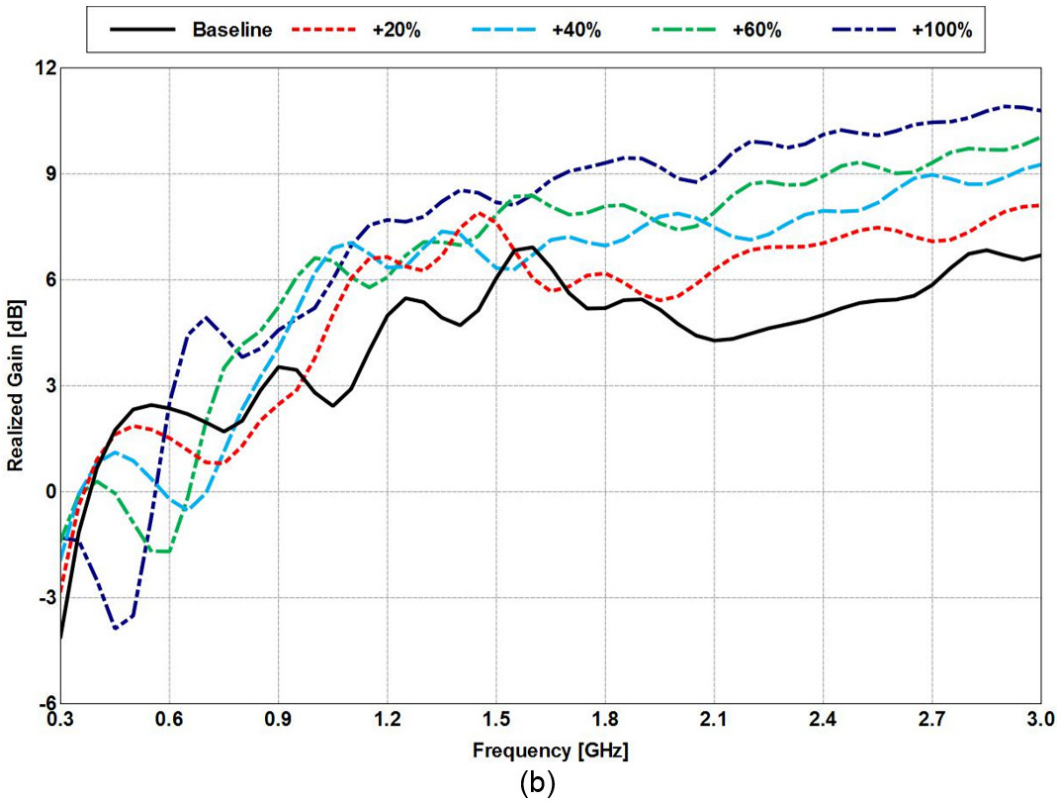

Fig. 11 Simulated a) reflection coefficient and b) realized gain vs. frequency for percentage increase in flare length and ending taper width (continued)

Figures 12a and 12b show the comparison between the BAV with a 60% longer flare and taper width and the Vivaldi-simulated reflection coefficient and realized gain vs. frequency. The final simulated design has a significant improvement in the impedance match, which will translate to a much better VSWR and either comparable or greater gain than the Vivaldi. A final change to the BAV was to reduce the substrate thickness so that it could be built using standard boards. Custom substrate thicknesses could be bought but would increase cost. The final design has a thickness of 0.25 inch instead of 0.3 inch. The reduced substrate thickness negatively effects the impedance match but improves the gain as shown in Figure 13a and 13b. The stripline width was adjusted to accommodate the change in substrate thickness. See the Appendix A for simulation results of the reduced-profile BAV performance versus substrate thickness and Appendix B for the BAV schematic.

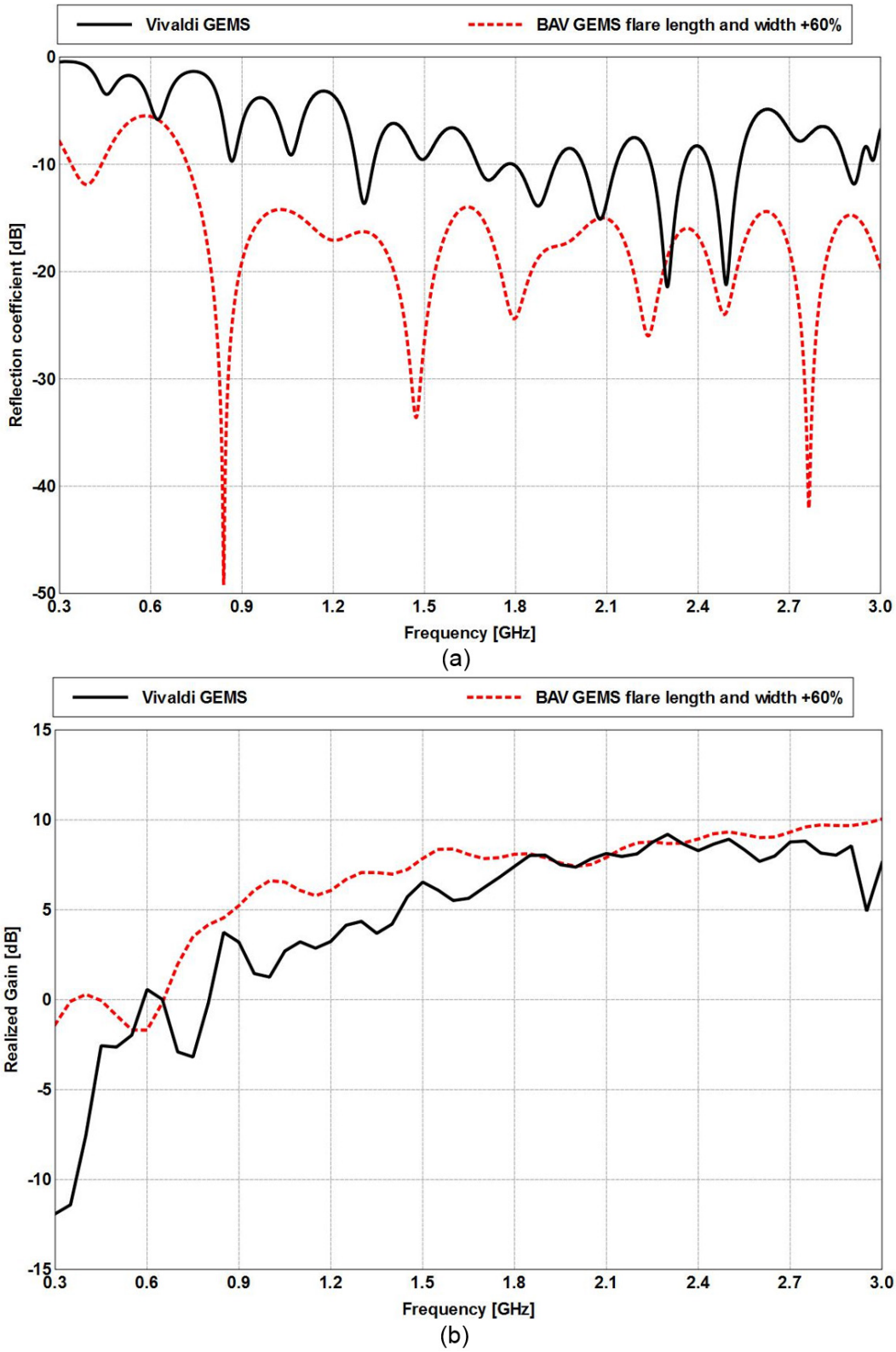

Fig. 12 Comparison of BAV with 60% longer flare and taper width and Vivaldi-simulated a) reflection coefficient and b) realized gain vs. frequency

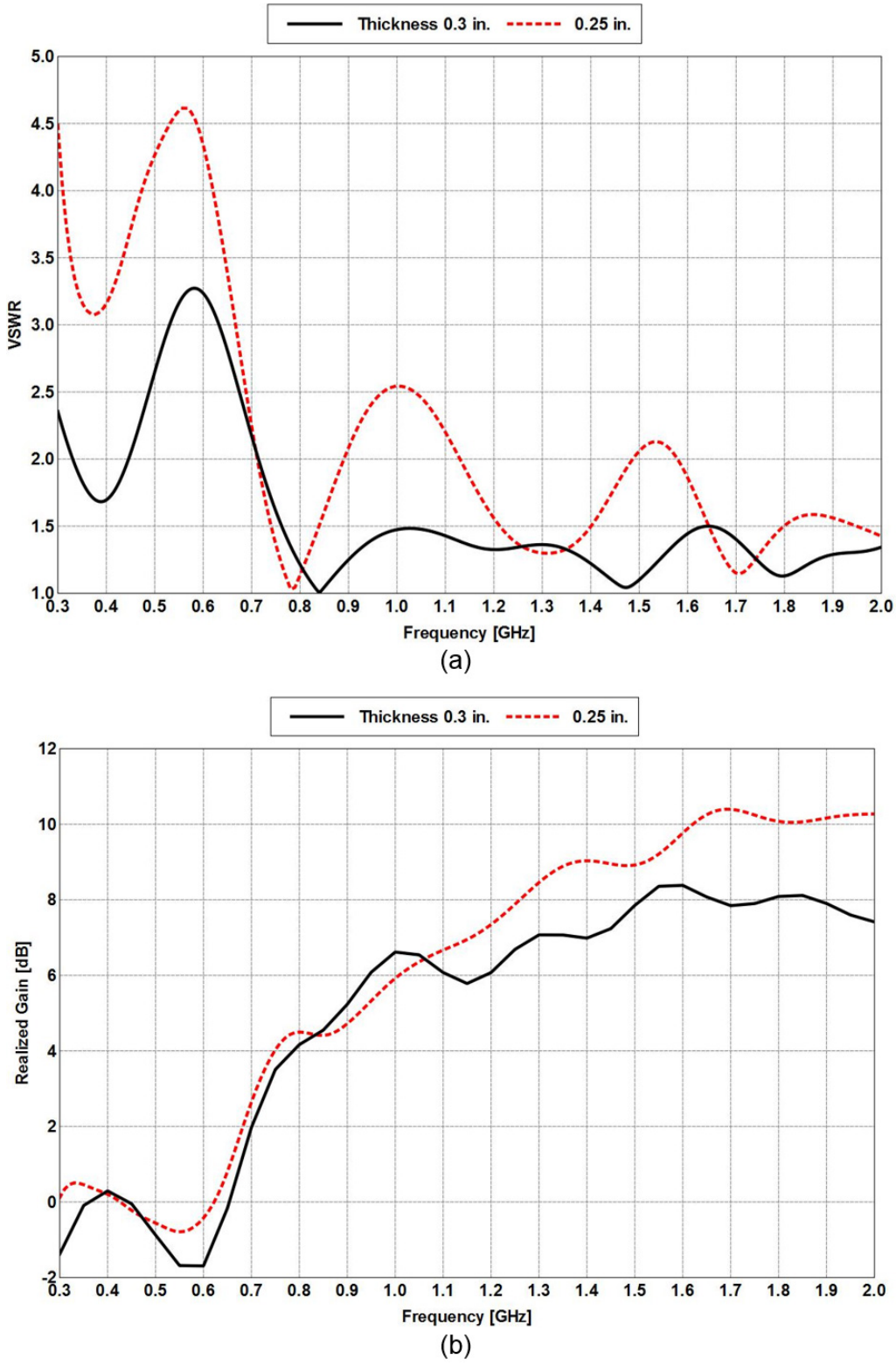

Fig. 13 Simulated a) VSWR and b) realized gain vs. frequency for the BAV with substrate thickness of 0.3 and 0.25 inch

5. BAV Measurement and Simulation Comparisons

This section shows the simulation and measurement comparisons for the fabricated BAV. Figures 14a and 14b show the measured and simulated VSWR and realized gain for the BAV and the measured results for the Vivaldi. The VSWR of the BAV is below 3.0 only for frequencies greater than 0.7 GHz. Below 0.7 GHz, the VSWR is as large as 5.0, but the Vivaldi VSWR is asymptotically large at those same frequencies. Except for 1.5–1.7 GHz and 1.8–2.0 GHz, the BAV has lower VSWR compared to the Vivaldi. The measured realized gain, Fig. 14b, confirms that the BAV has up to 8 dB more gain below 0.5 GHz and up to 5 dB more gain above 0.7 GHz. Between 0.5 and 0.7 GHz, the gain is comparable to the Vivaldi. Gain measurements with 2 different horns were required to cover 0.3–2.0 GHz. The data name "BAV Previous Measurement" was taken using a ridged SATIMO horn, which is spec'd to cover 0.4–6.0 GHz. It gives the best results, as it is small enough to be placed in the back of the tapered anechoic chamber apex. The data above 1.8 GHz are spurious because of chamber effects.

The other 4 measurements were taken with a ridged horn spec'd from 0.18 to 2.15 GHz. Because of the horn's size, it had to be positioned far out of the chamber apex, which worsened the spurious data points in the gain measurements. The E- and H-plane realized gains were taken to observe polarization dependencies of the artifacts. The 2 data sets were averaged together in linear space to attempt to average out some of the artifacts, but there are still serious spurious data points particularly between 1.3 and 1.7 GHz, where the gain is measured to be up to 2 dB lower than the previous measurement with the SATIMO. The low-frequency gain is in good agreement with simulation, confirming the improved gain, albeit with some inaccurate data.

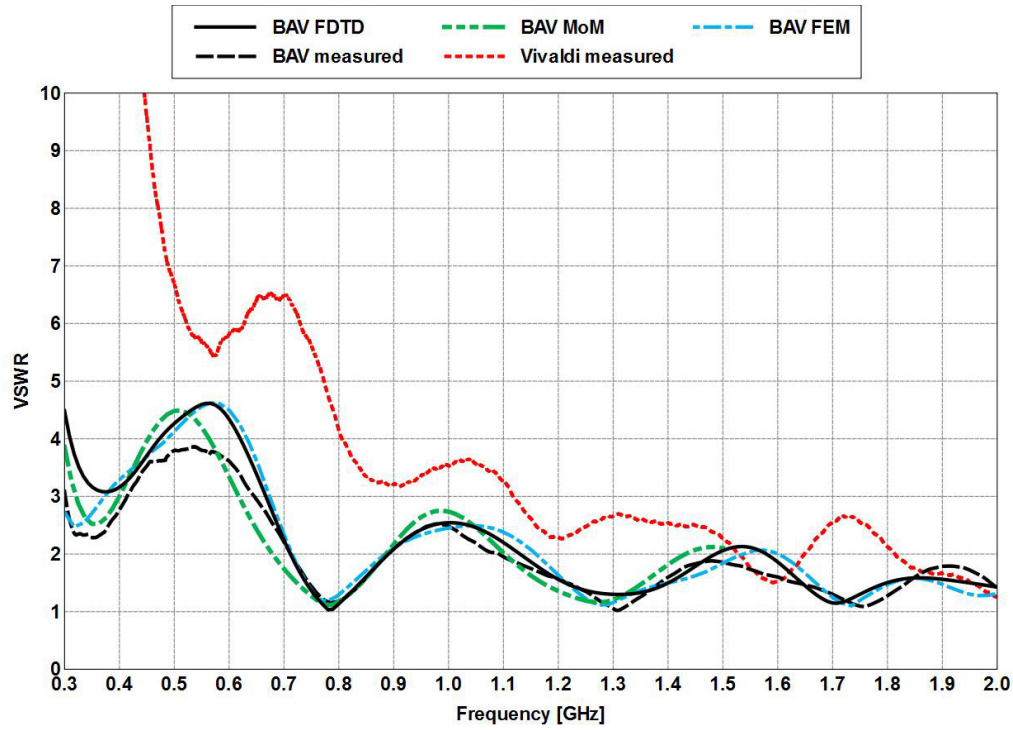

(a)

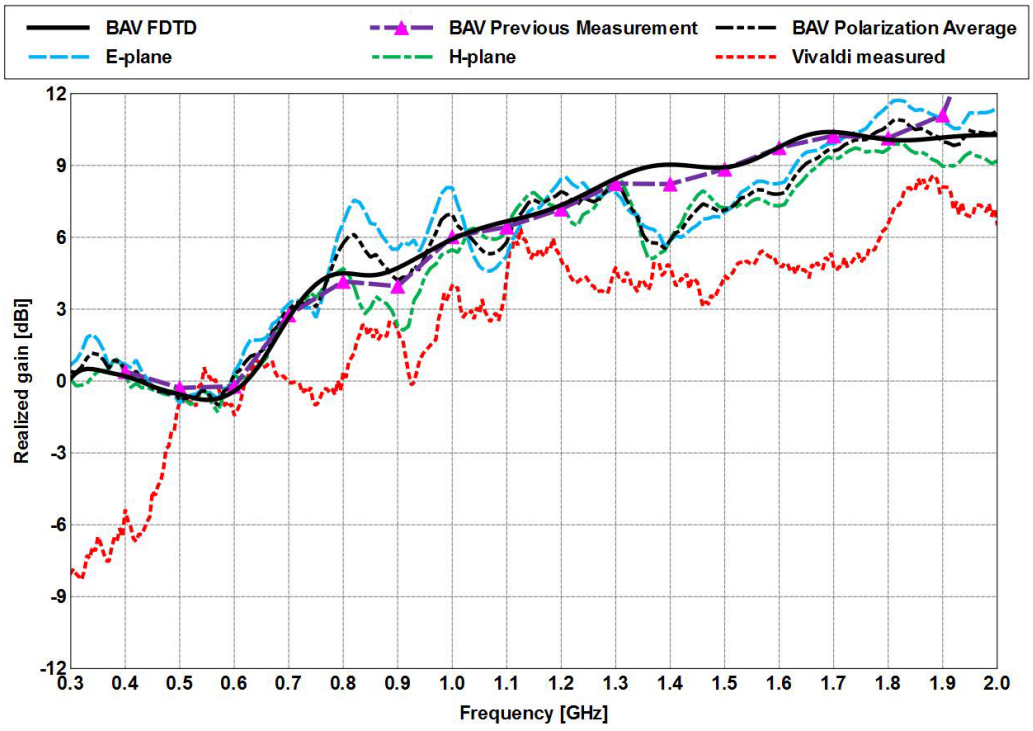

(b)

Fig. 14 Comparison of simulated and measured a) VSWR and b) realized gain vs. frequency for the BAV and Vivaldi

Figures 15a–c show the comparison of the simulated and measured realized gain patterns at 0.3, 0.7, 1.5, and 2.0 GHz. The data and simulations are in good agreement. The measurements confirm a dipole-like radiation pattern at 0.3 GHz with a more directive pattern at frequencies greater than 0.4 GHz. The radiation pattern is stable in the H-plane, but the E-plane pattern shows a tendency to favor the side with 2 fins in the mid band and comes back to the forward direction at high frequencies. The F/B of the BAV, Fig. 16a, becomes greater than 2 dB above 0.5 GHz and is up to 11 dB larger than the Vivaldi F/B for almost the entire frequency band. The 3-dB beamwidths, Fig. 16b, show that the BAV has a slower reduction with increasing frequency as compared to the Vivaldi. The frequency range covers only 0.7–2.0 GHz as both antennas start to approach beamwidths of greater than 180° below 0.7 GHz. Figure 16c shows the simulated normalized transient response for the BAV and Vivaldi, respectively. The results show that the BAV has reduced late time ringing compared to the Vivaldi, which would be ideal for a pulsed or even for stepped frequency systems, such as the FLGPR system the BAV is designed for. Removing the short metallic sides on the Vivaldi does not help the late time ringing, but removing the duplicate tapered slot side does help as shown in Fig. 16c. Still, the Vivaldi has larger late time ringing than the BAV.

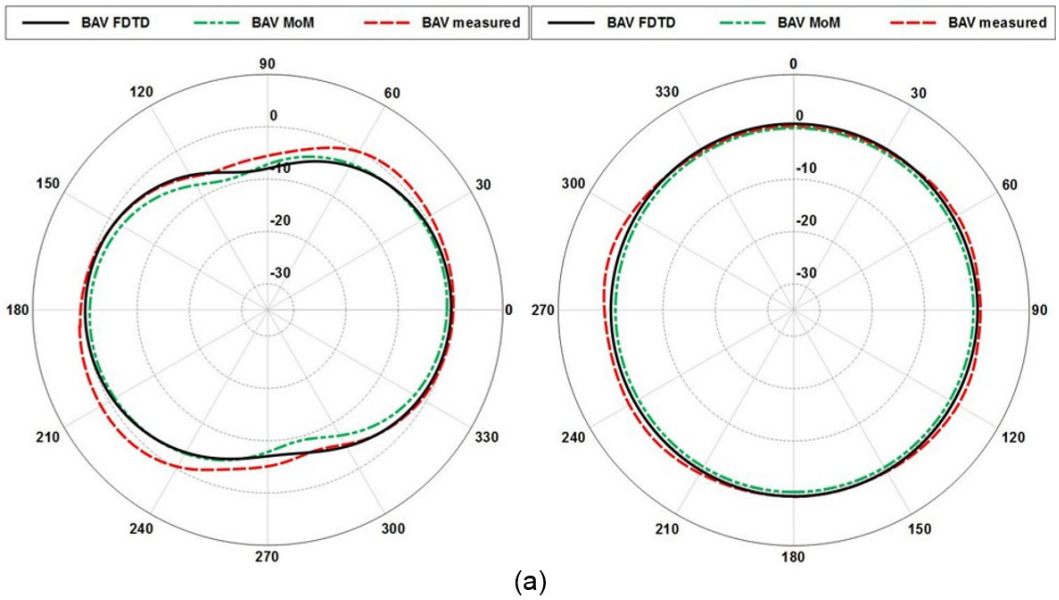

Fig. 15 Simulated and measured realized gain patterns for the BAV at a) 0.3 GHz, b) 0.7 GHz, c) 1.5 GHz, and d) 2.0 GHz. E-plane is on the left and H-plane is on the right.

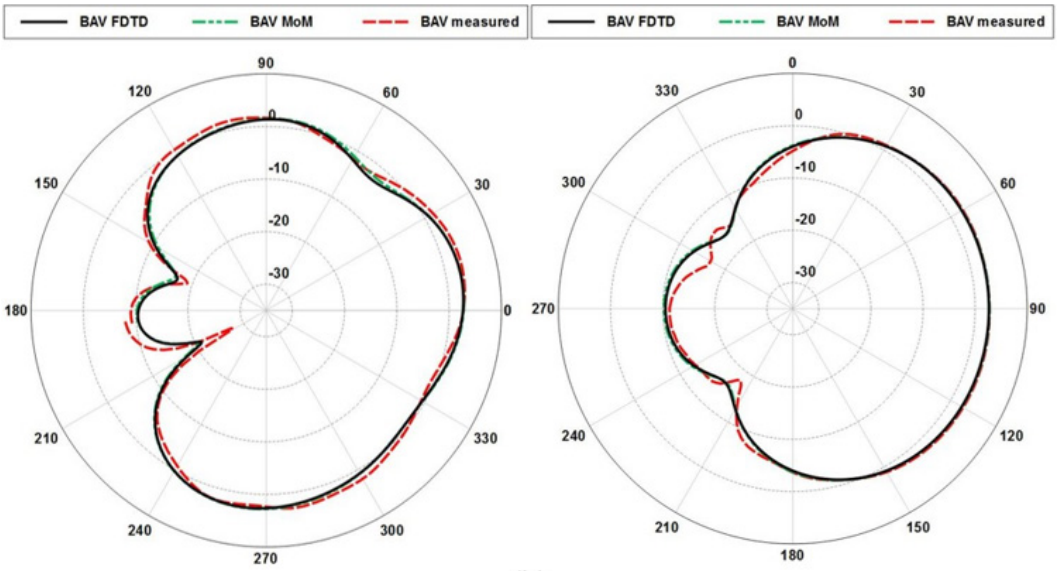

(b)

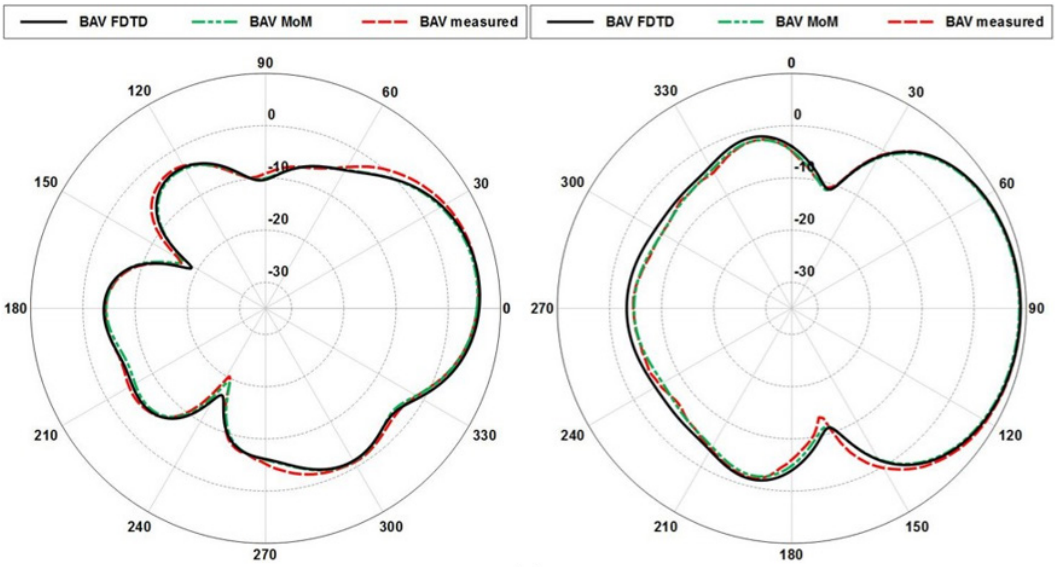

(c)

Fig. 15 Simulated and measured realized gain patterns for the BAV at a) 0.3 GHz, b) 0.7 GHz, c) 1.5 GHz, and d) 2.0 GHz. E-plane is on the left and H-plane is on the right (continued).

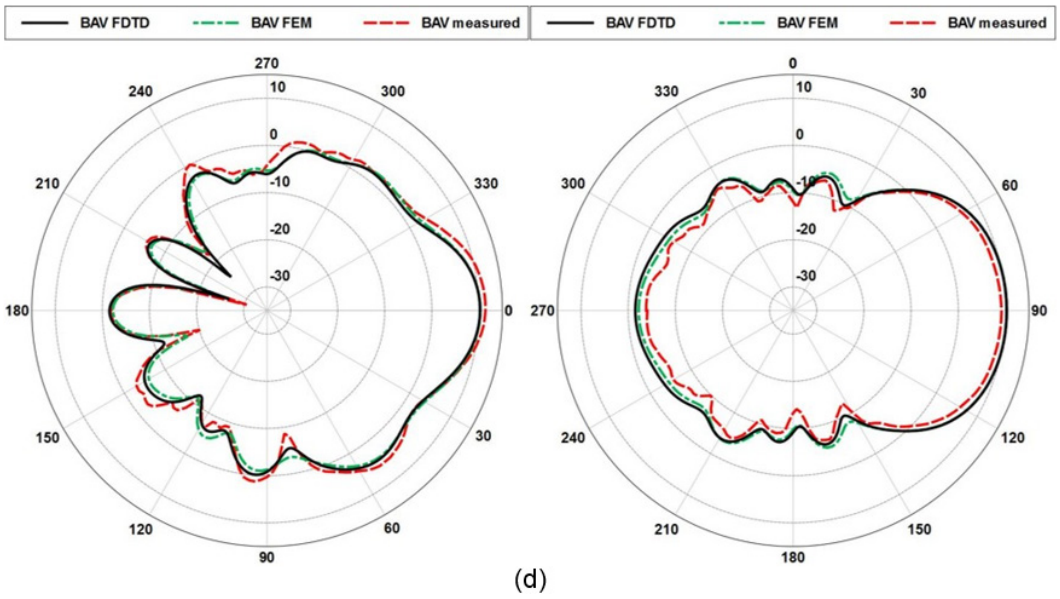

Fig. 15 Simulated and measured realized gain patterns for the BAV at a) 0.3 GHz, b) 0.7 GHz, c) 1.5 GHz, and d) 2.0 GHz. E-plane is on the left and H-plane is on the right (continued).

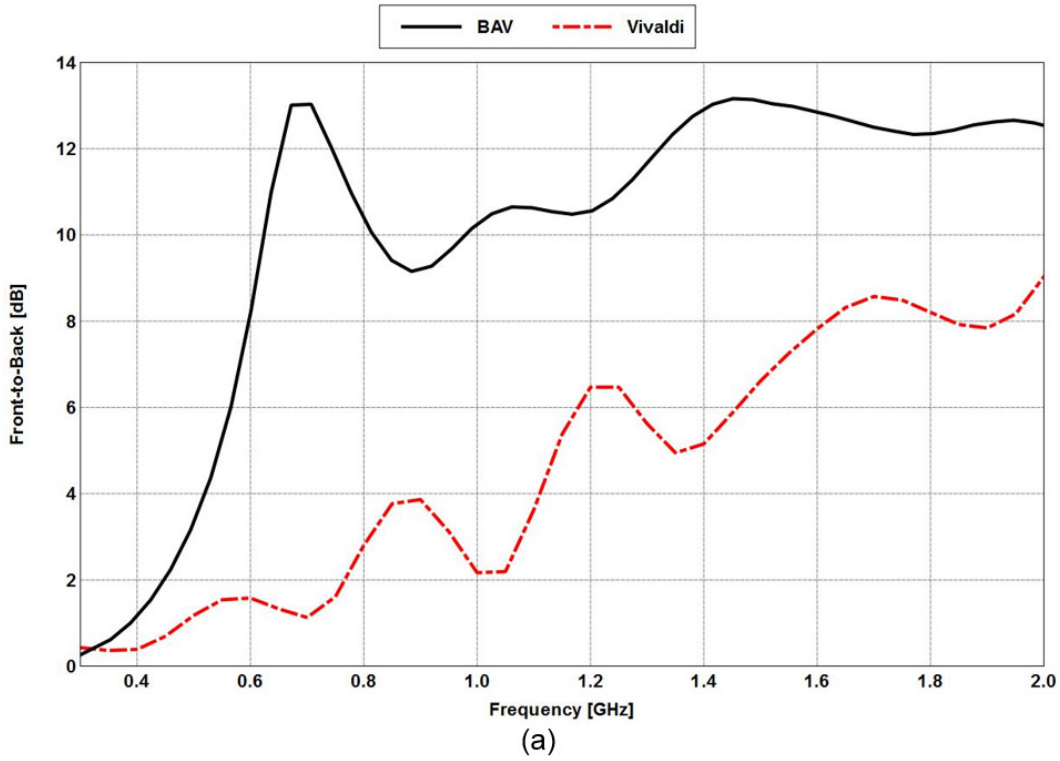

Fig. 16 Comparison of simulated a) F/B, b) 3-dB beamwidth, and c) normalized transient response for the BAV and Vivaldi

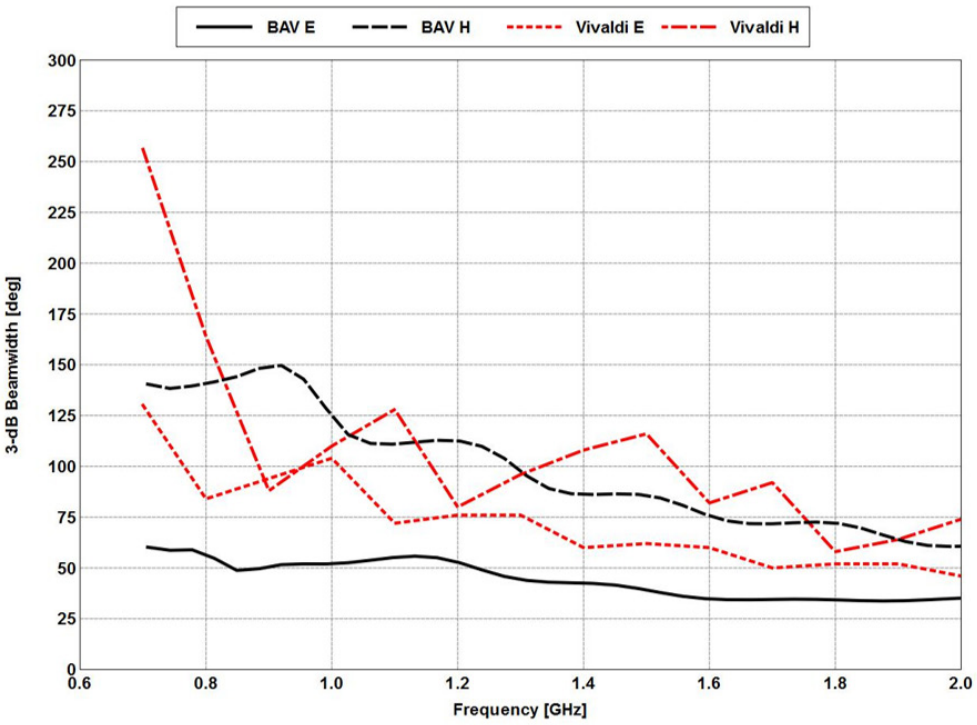

(b)

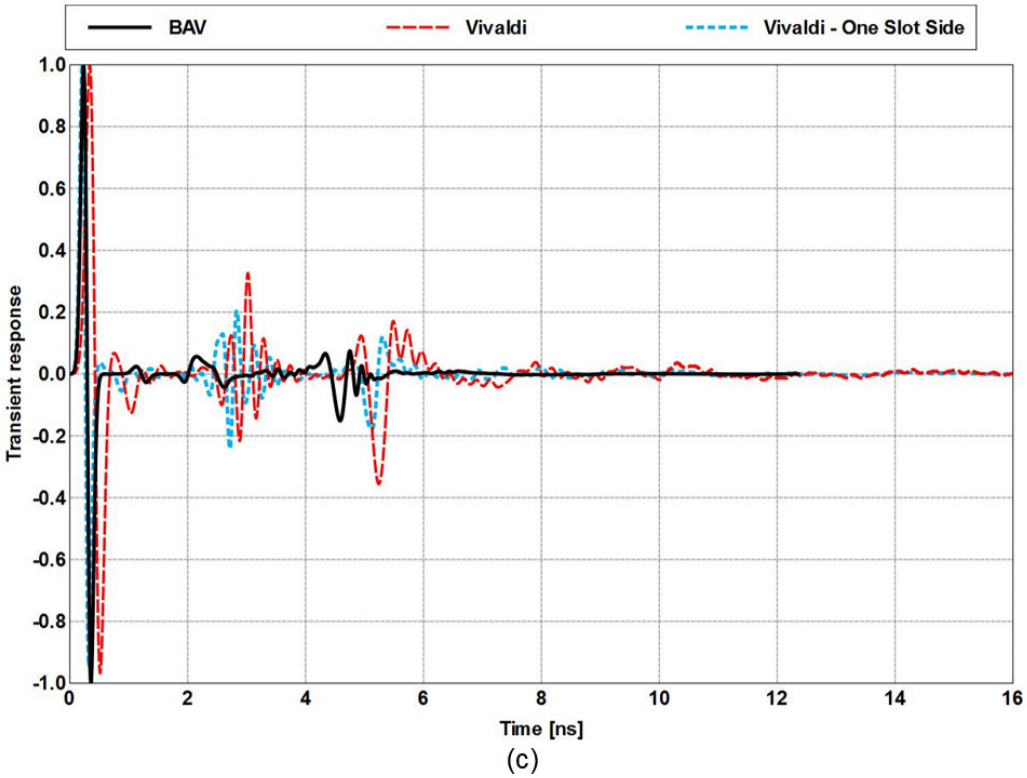

(c)

Fig. 16 Comparison of simulated a) F/B, b) 3-dB beamwidth, and c) normalized transient response for the BAV and Vivaldi (continued)

6. Simulations and Measurements of BAV Pairs

This section presents the simulated and measured reflection coefficient, realized gain, and cross-pol isolation between pairs of BAV elements to determine position-dependent coupling effects on individual element performance as well as to maximize cross-pol isolation. Simulation tools were leveraged after model validation in lieu of measurements to ensure that performance effects were dictated by antenna-to-antenna interactions and not the environment. Cross-pol isolation was measured for validation to ensure accuracy as the simulation environment is idealized. Figure 17a shows the recommended configuration for 32 BAV receivers to minimize the overall width dimension. The center-to-center element spacing is 0.5 inches, Figure 17b, which gives an overall height of 21.2 inches, a depth of 17.2 inches, and a width of 86.7 inches, which is within 2.2 m. The fin matching for the cross-pol elements was not initially considered and was found to be preferred to maintain antenna performance through simulating the different paired geometries. Figure 18 shows the 9 paired combinations. Pairs with matching fins have one antenna excited and the other terminated into 50 Ω, resulting in only one simulation. Pairs that do not have matching fins are simulated twice, interchanging the excitation and termination between the pair.

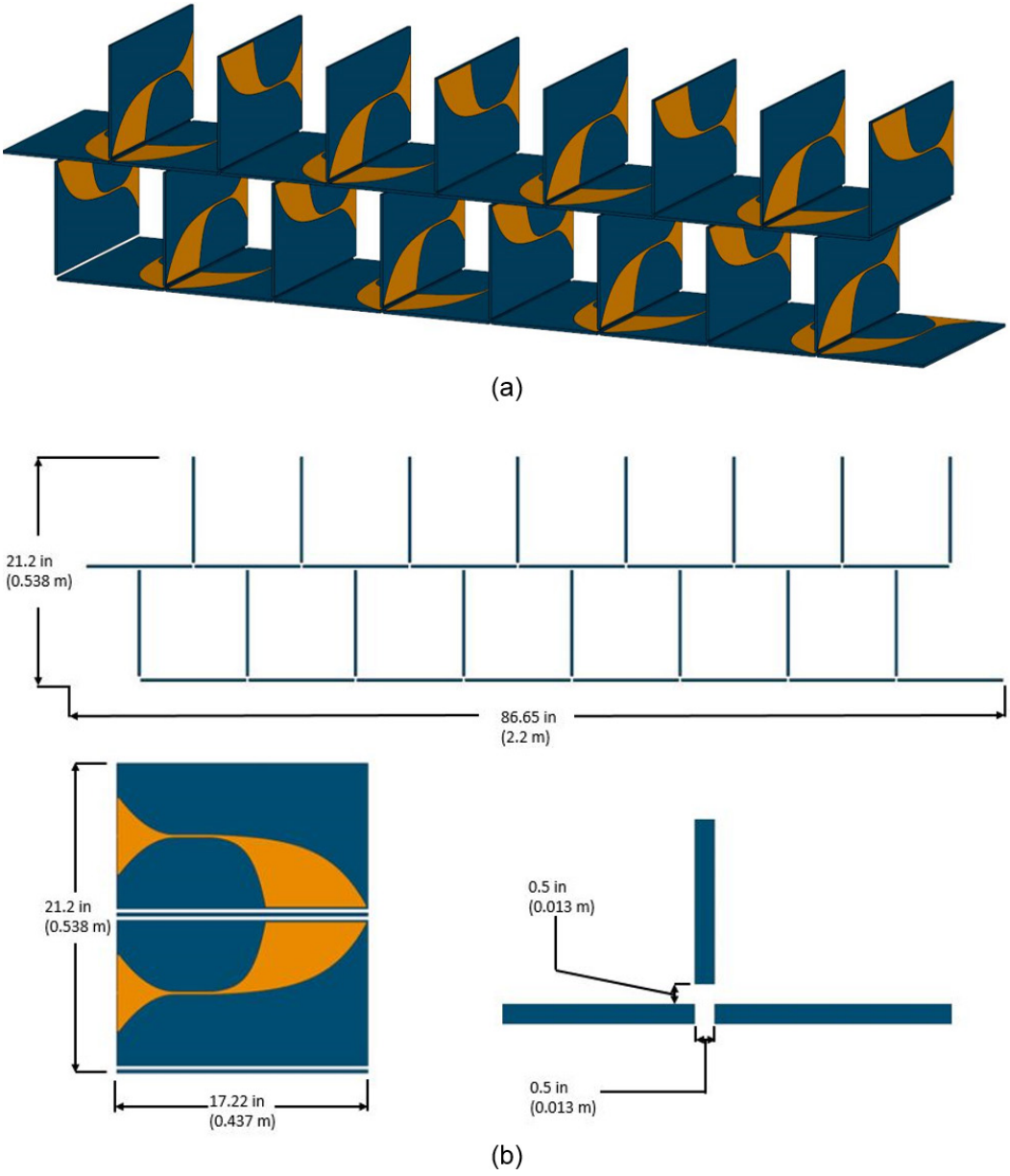

Fig. 17 Recommendation for a) receiver positioning to minimize width with b) element spacing and overall dimensions

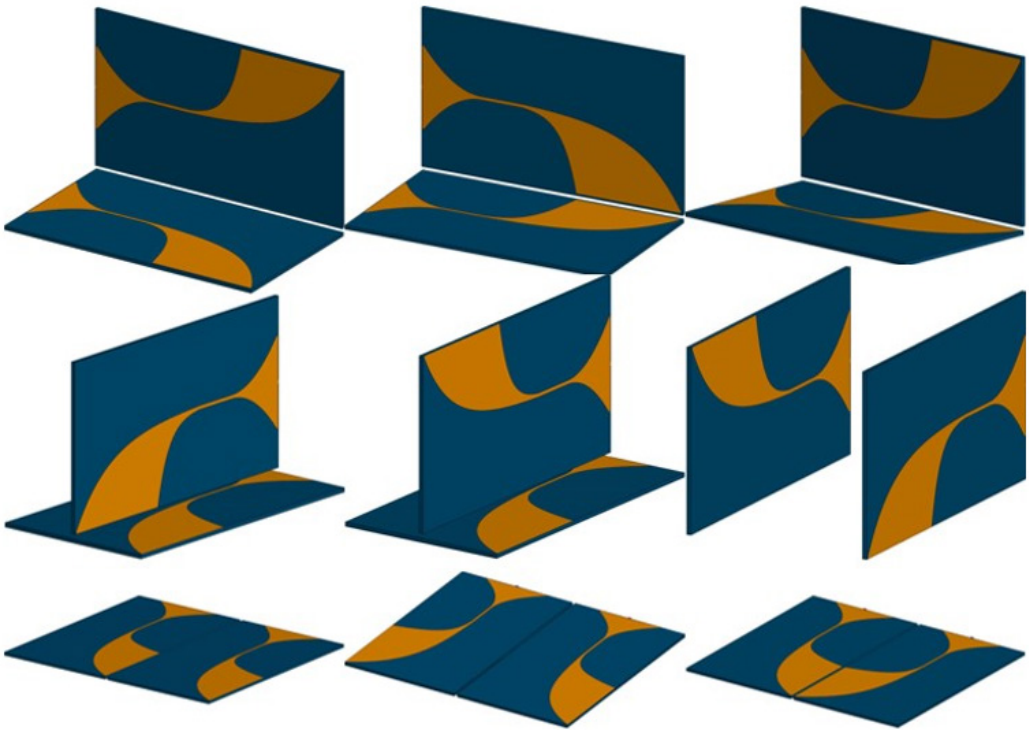

Fig. 18 CAD models for the BAV receiver pairs

Figure 19a shows the simulated reflection coefficient for the side-by-side vertical pair. Since the pair are mirror opposites of each other, only one simulation was performed. As can be seen by the reflection coefficient and the realized gain, Fig. 19b, this configuration has little effect on both the impedance match and realized gain. The biggest impact is on the 0.3-GHz realize gain, where the pair shows a 1-dB reduction. The F/B, Fig. 19c, shows that there is a decrease in the back lobe, which improves the F/B up to 1.1 GHz. The cause of the 7-dB improvement in the F/B at 0.7 GHz is shown in the H-plane radiation pattern, Fig. 19d. The side-by-side vertical arrangement has produced a null in the back lobe, which improves the F/B. The vertical configuration does not produce any observable negative performance effects that are of concern beyond the 1-dB gain loss at 0.3 GHz.

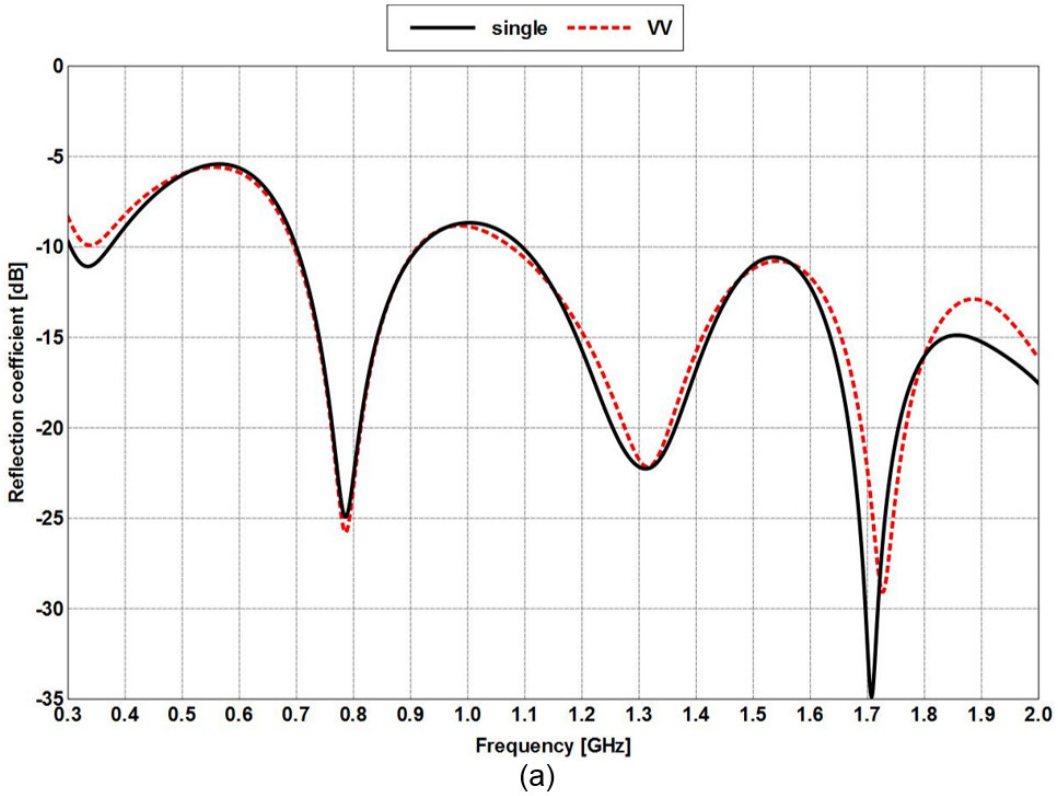

(a)

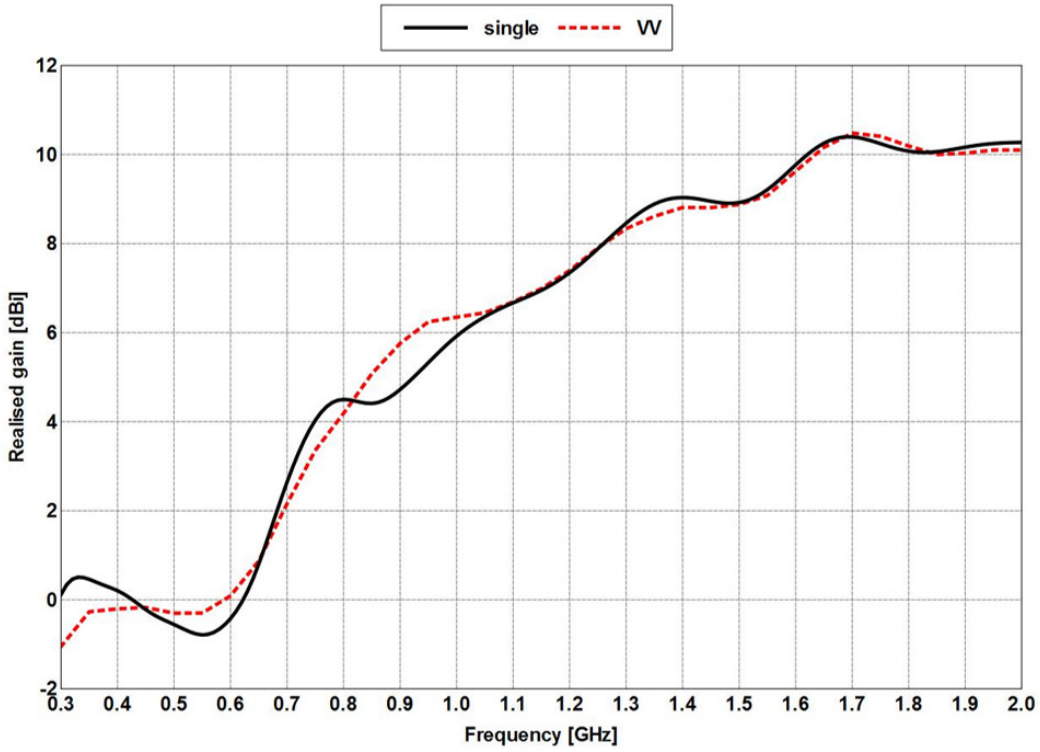

(b)

Fig. 19 Simulated a) reflection coefficient, b) realized gain, c) F/B, and d) 0.7-GHz H-plane pattern for the side-by-side vertical BAV pair

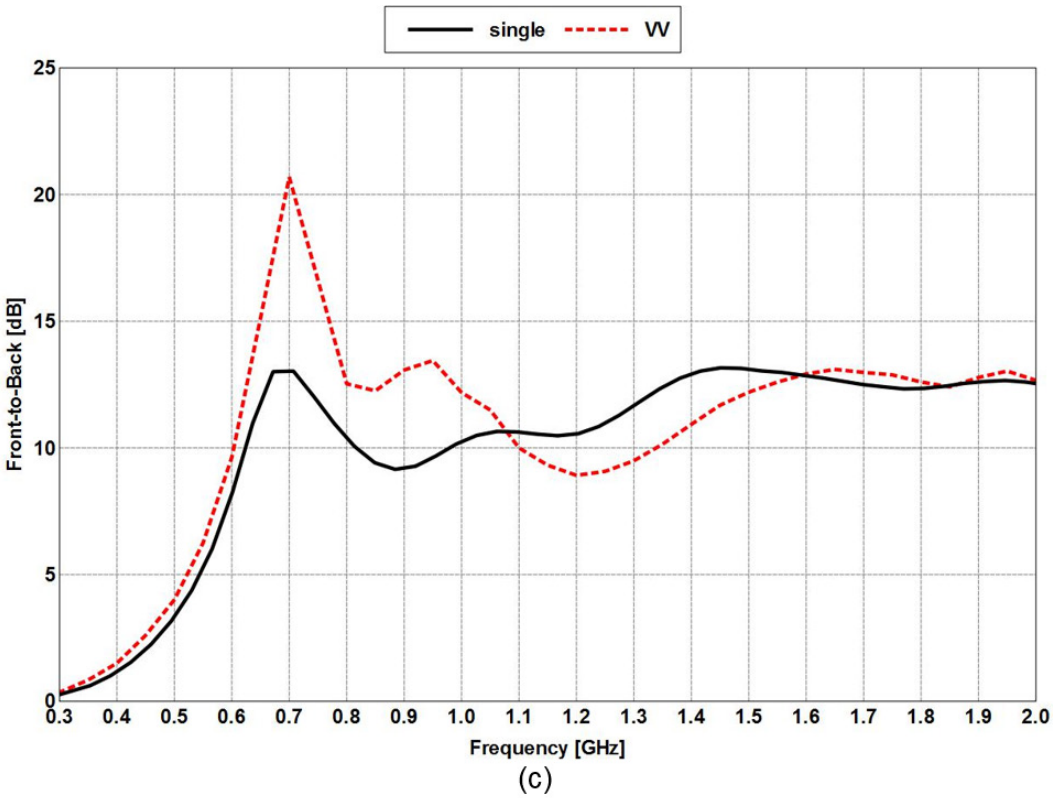

(c)

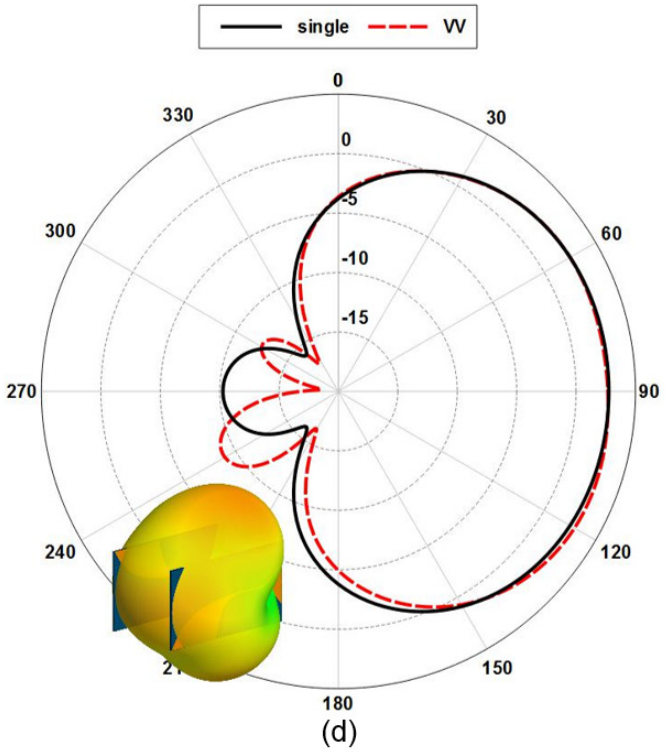

(d)

Fig. 19 Simulated a) reflection coefficient, b) realized gain, c) F/B, and d) 0.7 GHz H-plane pattern for the side-by-side vertical BAV pair (continued)

Simulated results for the side-by-side horizontal pair are shown in Figs. 20a–c. The naming convention is as follows: The term "gnd" means that grounded fins are next to each other; "hot" refers to center fins next to each other; "flipped" refers to a grounded fin next to a center fin; "left" and "right" refer to which BAV is excited. Directional reference is taken to be in the direction of propagation. From the simulated reflection coefficient, Fig. 20a, the gnd, hot, and flipped left configurations show similar results, although the flipped-left case has the poorest impedance match below 0.4 GHz. The flipped-right configuration shows that the reflection coefficient is significantly influenced by the antenna to the left. The realized gain, Fig. 20b, shows a similar trend. The forward realized gain is similar for the gnd, hot, and flipped-left configurations, but the flipped-right simulation shows degraded realized gain above 1.0 GHz. There is more variation between the 4 cases in the F/B, Fig. 20c. The hot and flipped-left simulations have similar F/B results but are different compared to the gnd and flipped right simulations. All 4 simulations show degraded F/B between 0.6 and 0.9 GHz and improved F/B above 1.8 GHz.

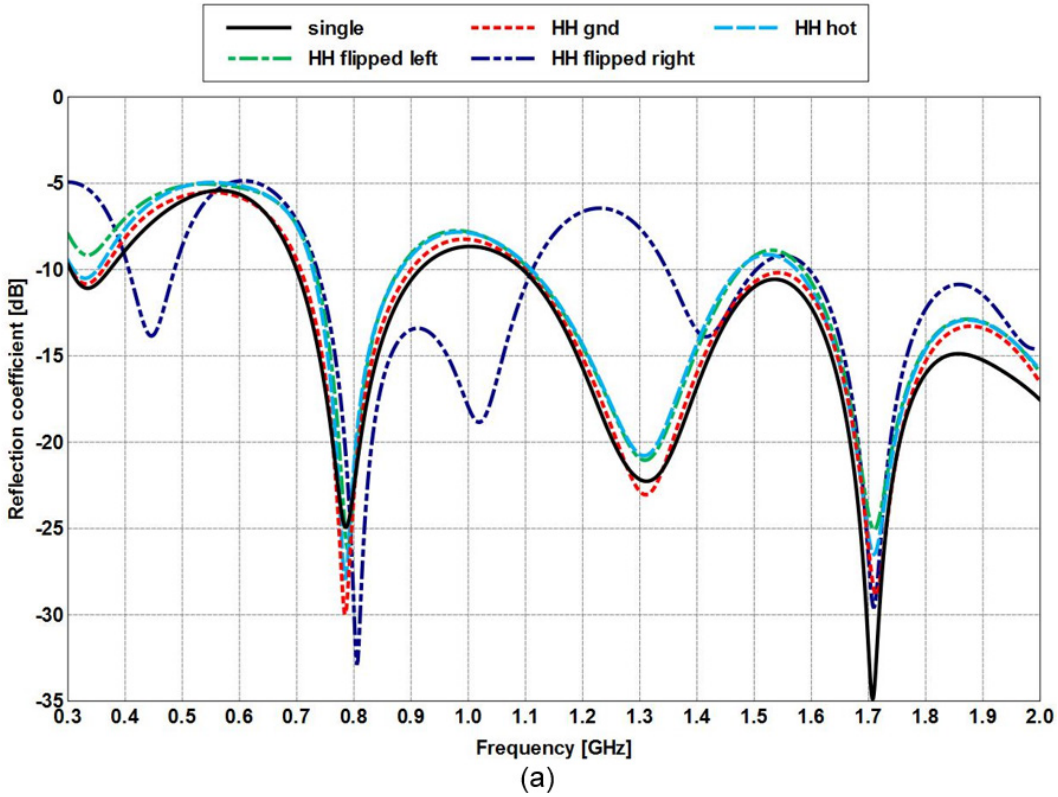

Fig. 20 Simulated a) reflection coefficient, b) realized gain, and c) F/B vs. frequency for the side-by-side horizontal BAV pair

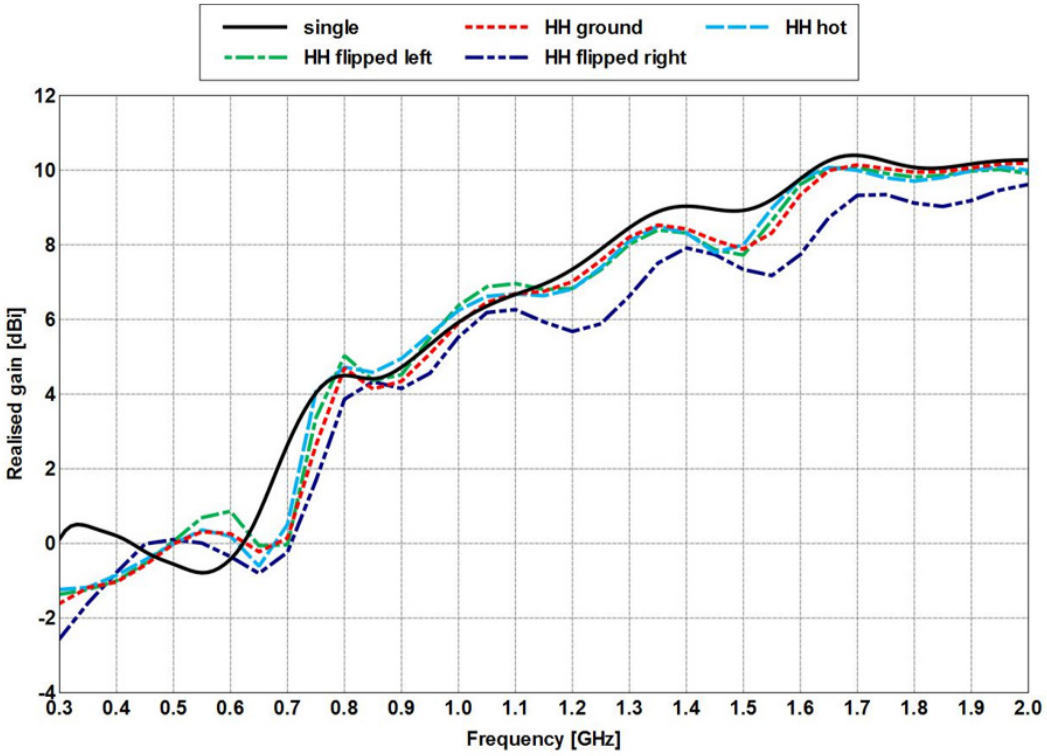

(b)

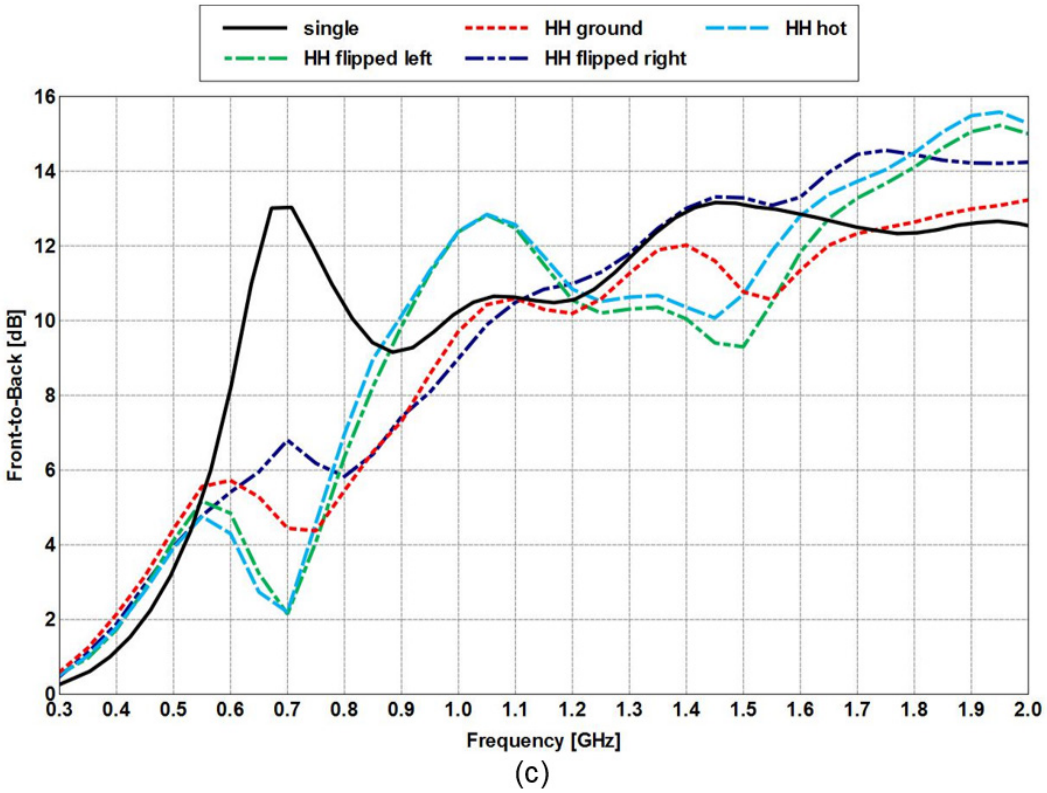

(c)

Fig. 20 Simulated a) reflection coefficient, b) realized gain and c) F/B vs. frequency for the side-by-side horizontal BAV pair (continued)

Simulated results for the centered dual-pol pair are shown in Figs. 21a–d. The naming convention is as follows: The term "flipped" refers to the vertical element with its grounded fins positioned toward the underlying horizontal element; "HV" and "VH" denote which antenna is excited and which is terminated; the first letter references the excitation and the second letter the termination. The centered configuration shows the greatest degradation in reflection coefficient besides the previous "flipped right" simulation, Fig. 21a, particularly below 0.6 GHz. The curves for the VH and flipped HV cases are also not as smooth as the other 2 with some additional local maxima and minima introduced. The realized gain, however, is not as poorly degraded, if at all, Fig. 21b. The F/B, Fig. 21c, has been significantly affected with the exception of the HV simulation. A 10-dB dip has been introduced between 0.6 and 0.7 GHz in the VH and flipped VH configurations, and a 4-dB increase has been introduced between 0.7 and 1.1 GHz in the VH configuration. The flipped HV has a 3-dB dip between 1.0 and 1.1 GHz and a 4-dB larger peak between 1.4 and 1.6 GHz. Between 1.7 and 2.0 GHz the flipped HV configuration sees the largest variation of all configurations.

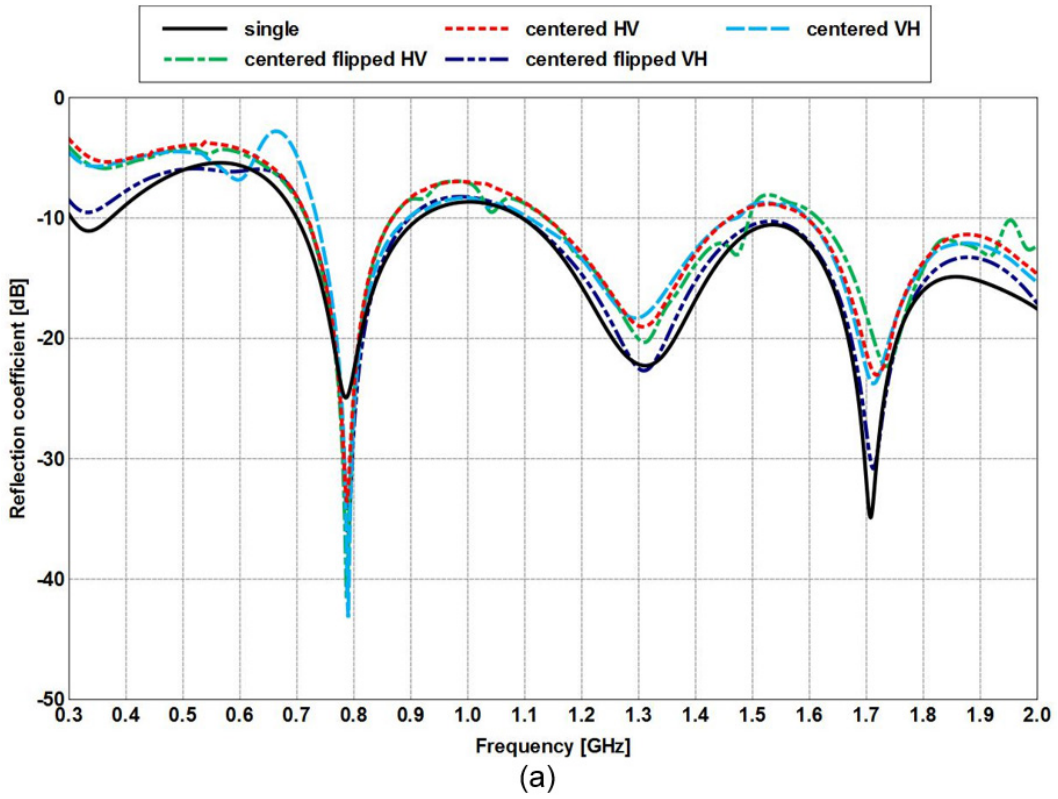

Fig. 21 Simulated a) reflection coefficient, b) realized gain, c) F/B, and d) cross-pol isolation vs. frequency for the centered dual-pol BAV pair

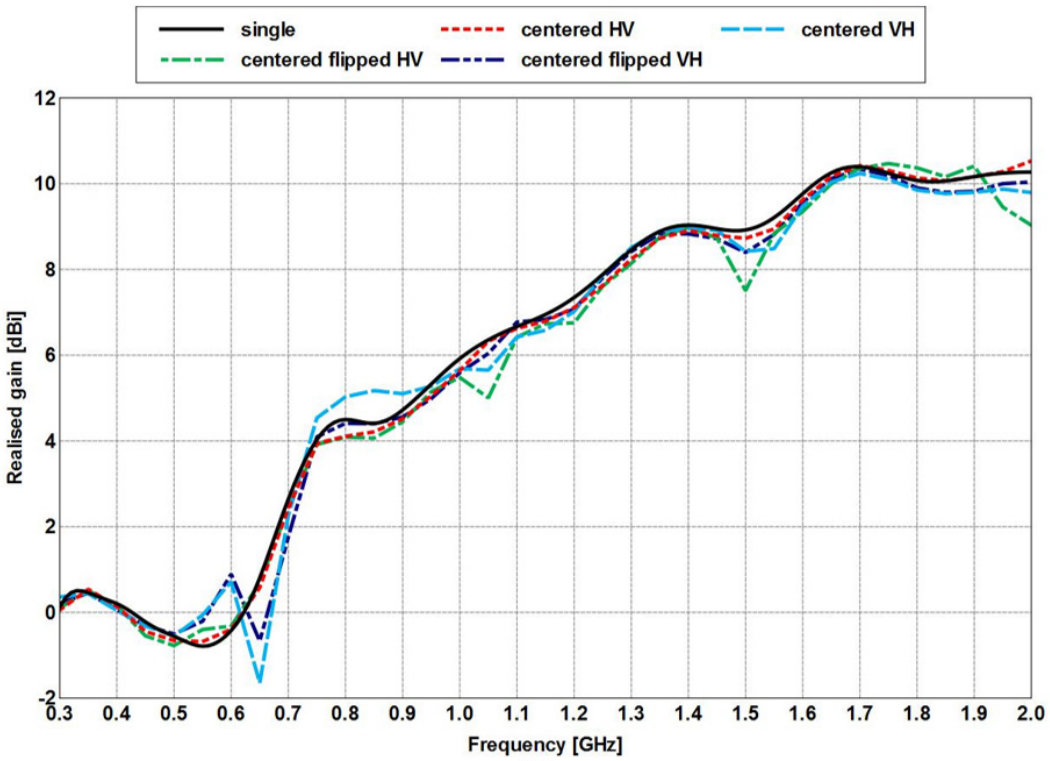

(b)

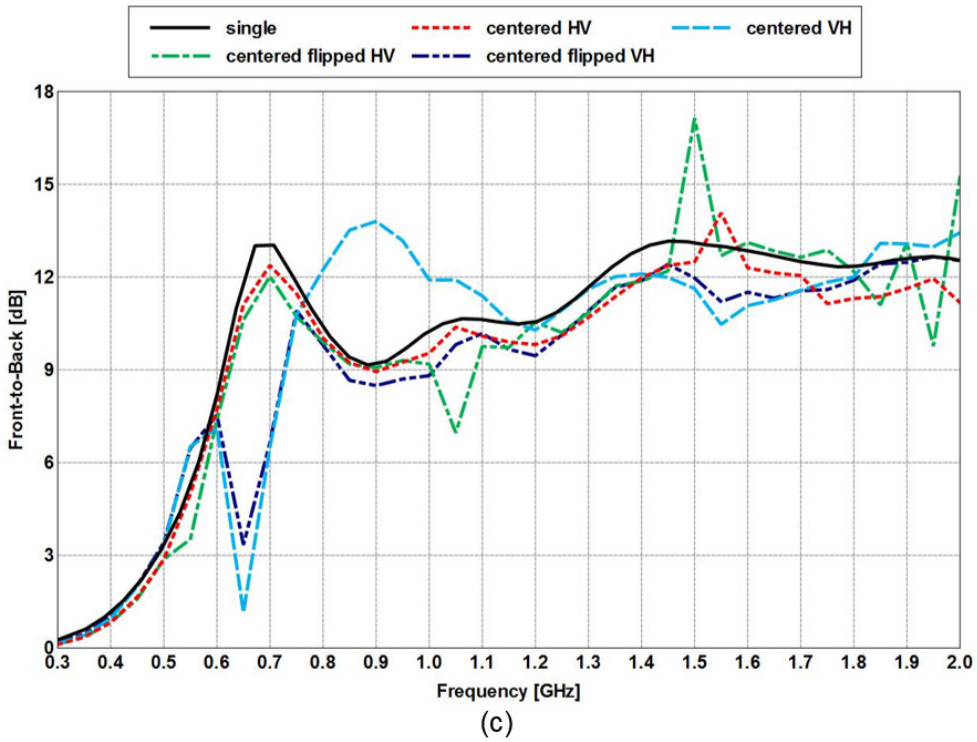

(c)

Fig. 21 Simulated a) reflection coefficient, b) realized gain, c) F/B, and d) cross-pol isolation vs. frequency for the centered dual-pol BAV pair (continued)

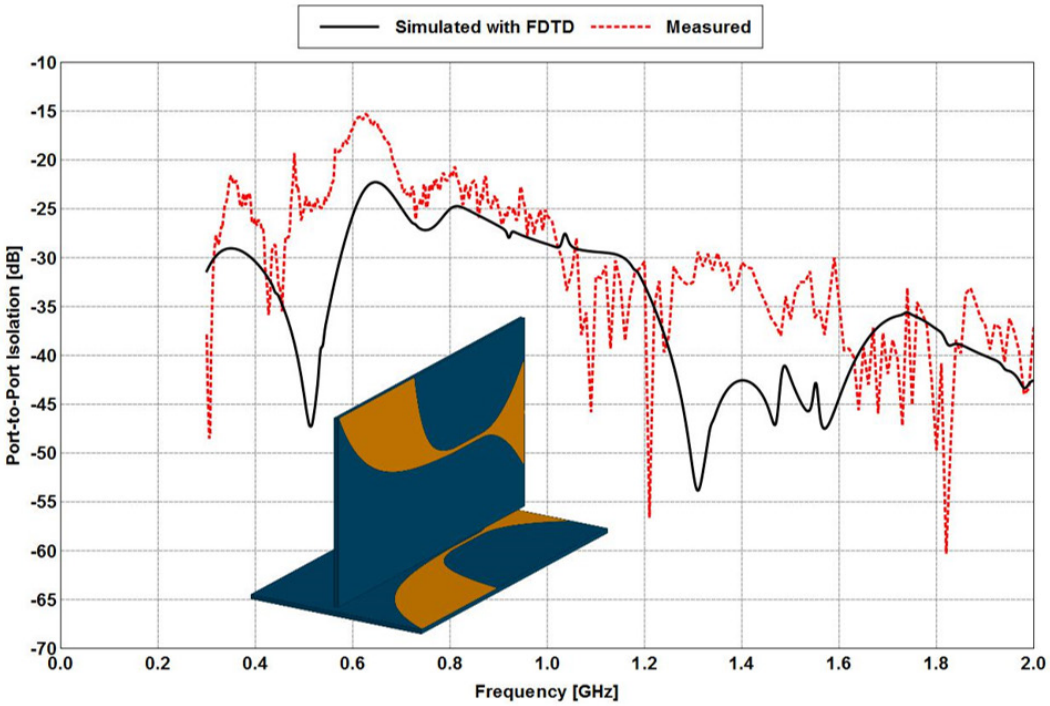

(d)

Fig. 21 Simulated a) reflection coefficient, b) realized gain, c) F/B, and d) cross-pol isolation vs. frequency for the centered dual-pol BAV pair (continued)

The simulated and measured cross-pol isolation is shown in Figure 21d. Simulations show 22 dB or greater isolation, but measurements show only 15 dB or better, the worse occurring between 0.6 and 0.65 GHz. It is important to note that the isolation measurement can be sensitive to the measurement environment. For that reason, the measurement was done within the onsite near-field measurement range where the walls are RF absorber lined. The absorber is not rated below L-band but can still reduce reflections from the walls. The anechoic room also has less metallic artifacts to produce reflections. For this reason, the centered configuration should be spec'd at 15-dB minimum isolation. The electric current distribution for the VH simulation at the dip frequency 0.65 GHz and peak frequency of 0.9 GHz in the F/B is shown in Fig. 22. There is a strong interaction between the center fin of the vertical element and the horizontal element beneath it at 0.65 GHz and a much weaker interaction at 0.9 GHz.

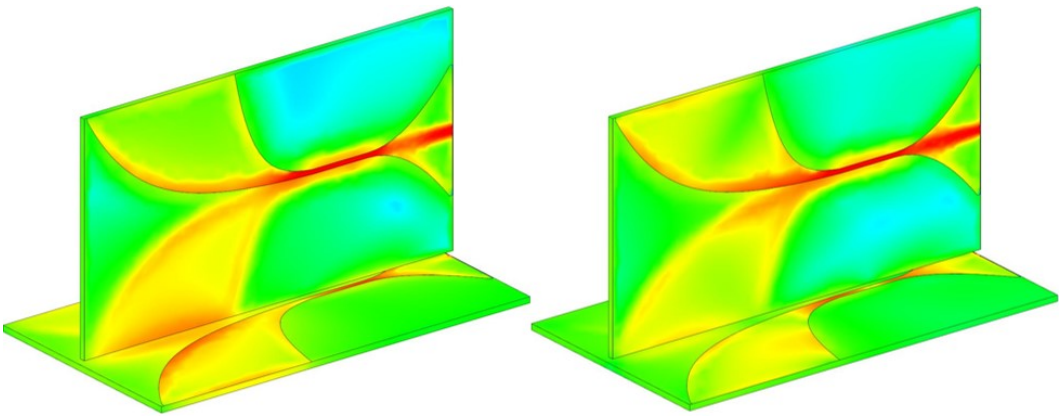

Fig. 22 Electric current for the "flipped VH" simulation at 0.65 and 0.9 GHz

Simulated results for the corner dual-pol pair are shown in Figs. 23a–c. The naming convention is as follows: "gnd" specifies that the grounded fins for the 2 antennas are next to each other; "hot" refers to side-by-side center fins; "flipped" refers to the grounded fin next to the center fin; "VH" and "HV" specify which antenna is excited and which is terminated, the same as the previous centered cases. Effects on the impedance match are mostly negligible for all cases except for the "corner flipped VH" configuration, which has the worst impedance match as seen from the simulated reflection coefficient, Fig. 23a. The realized gain, Fig. 23b, shows that the gain remains virtually unchanged for all frequencies above 0.6 GHz. Below 0.6 GHz, the gain is reduced by 0.5–1.0 dB because of the impedance match at those frequencies. Again, the flipped VH case has the poorest gain. The largest gain reduction is 1 dB at 0.3 GHz. The F/B is affected similarly amongst all configurations, Fig. 23c. Above 0.8 GHz, the F/B above the 4 configurations are within 1–2 dB of the single BAV, but they all lose up to 5 dB or more between 0.55 and 0.8 GHz.

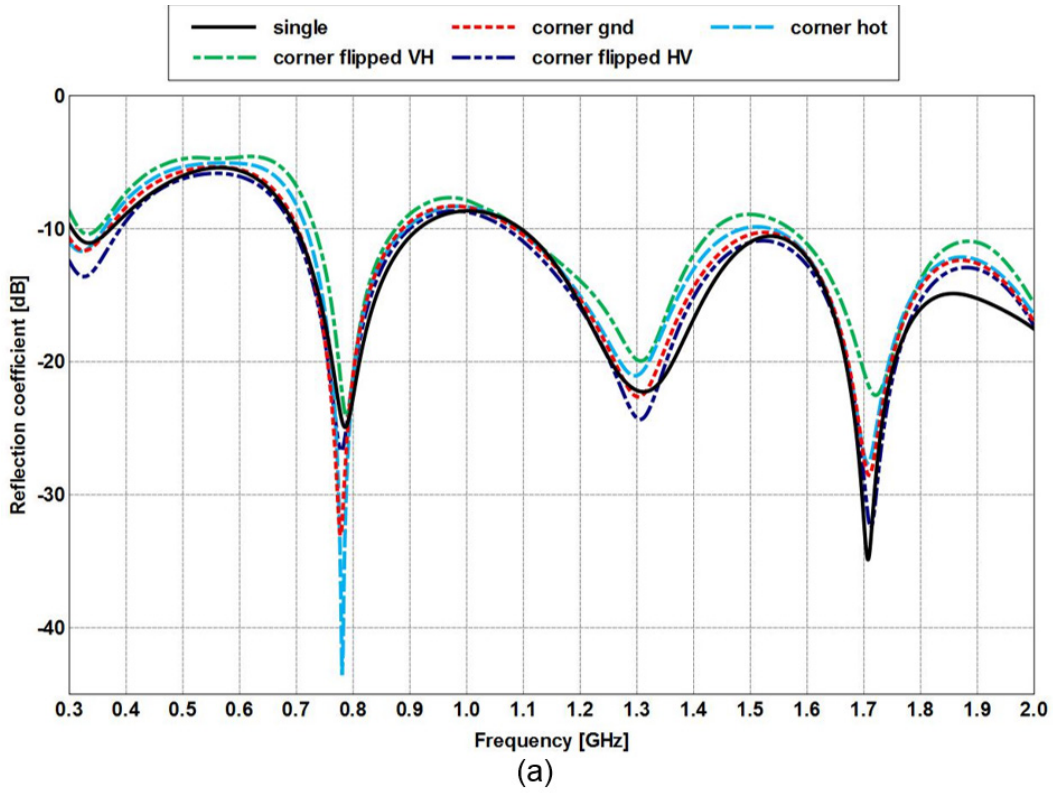

(a)

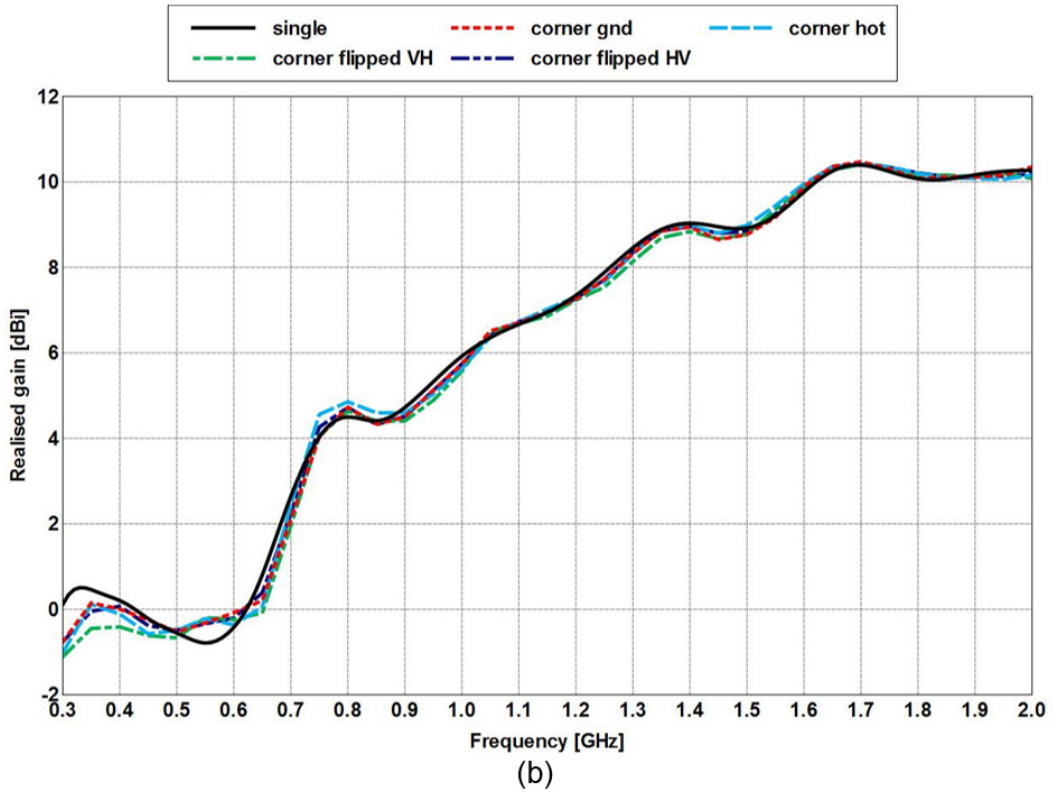

(b)

Fig. 23 Simulated a) reflection coefficient, b) realized gain, and c) F/B vs. frequency for the corner dual-pol BAV pair

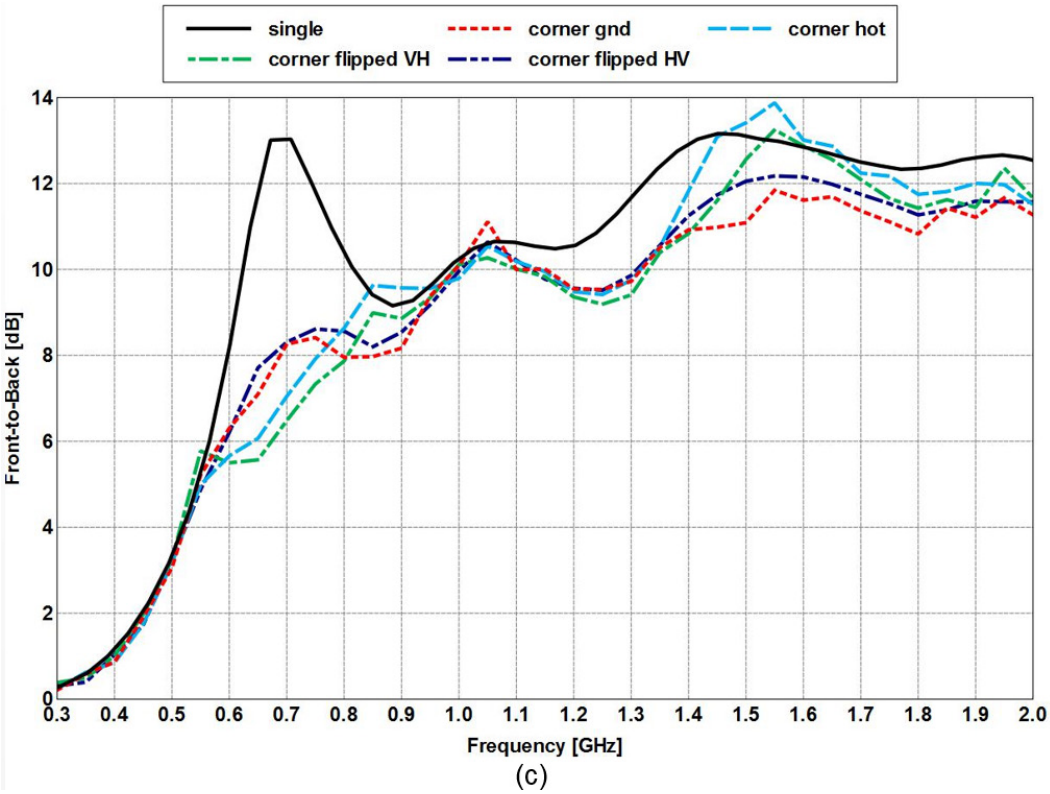

Fig. 23 Simulated a) reflection coefficient, b) realized gain, and c) F/B vs. frequency for the corner dual-pol BAV pair (continued)

A critical question to answer pertaining to the 32 element aperture was whether all of the BAV elements needed to be electrically connected together, and if so, what effect on performance would electrically connecting them have? It is suggested in the literature that nearby tapered slot antennas that are not connected can have reduced performance due to radiation from neighboring edge currents between the fins, and that electrically connecting the fins can reduce such effects.[11] A pair of BAV elements were built, as shown in Fig. 24a, to test performance effects caused by electrically connecting and disconnecting the neighboring fins for the "corner" configurations. Measurements of the reflection coefficient, realized gain, and cross-pol isolation were made and compared to simulation with the elements both soldered together at the grounded fins and disconnected. The same element positioning and spacing were maintained for both measurements. To connect the 2 elements, one of the BAV elements had a notch removed from one layer of the substrate so that the other BAV could rest on top. A copper strip was placed in between the newly formed right angle joint overlapping the grounded fins of both elements and connected with a continuous solder joint. In simulation, the PEC surfaces are joined by a perfect connection.

The simulated and measured reflection coefficient results are shown in Fig. 24b. The terms “C” and “NC” stand for connected and not connected, respectively. Agreement between simulation and measurement is not exact, particularly above 1.1 GHz; however, the trend between simulations and the trend between measurements are in agreement. That is, electrically connecting the elements has little effect on the impedance match as compared to not connecting them. The same is true for the realized gain shown in Fig. 24c. The dual-pol measurements have similar if not the same chamber artifacts as the lone BAV. Electrically connecting the elements does have an appreciable effect in the mutual coupling shown by the isolation data in Fig. 24d. Not connecting the elements can improve the cross-pol isolation by up to 10 dB at frequencies above 1.2 GHz, 5–10 dB between 0.6 and 1.2 GHz, and a modest improvement of 1–2 dB below 0.6 GHz.

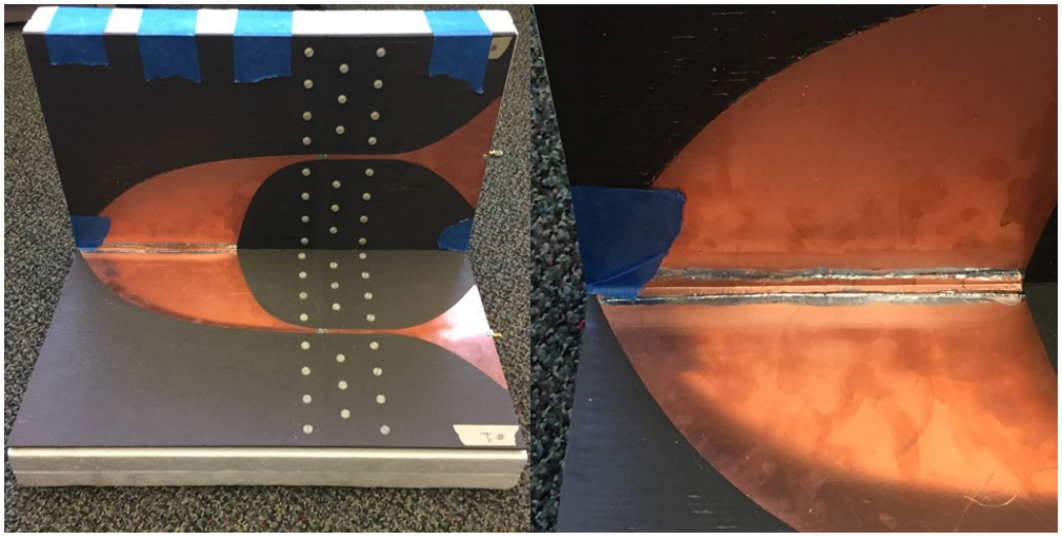

(a)

Fig. 24 a) Built corner dual-pol BAV pair, b) simulated and measured reflection coefficient, c) realized gain, d) cross-pol isolation vs. frequency, and e) transient response

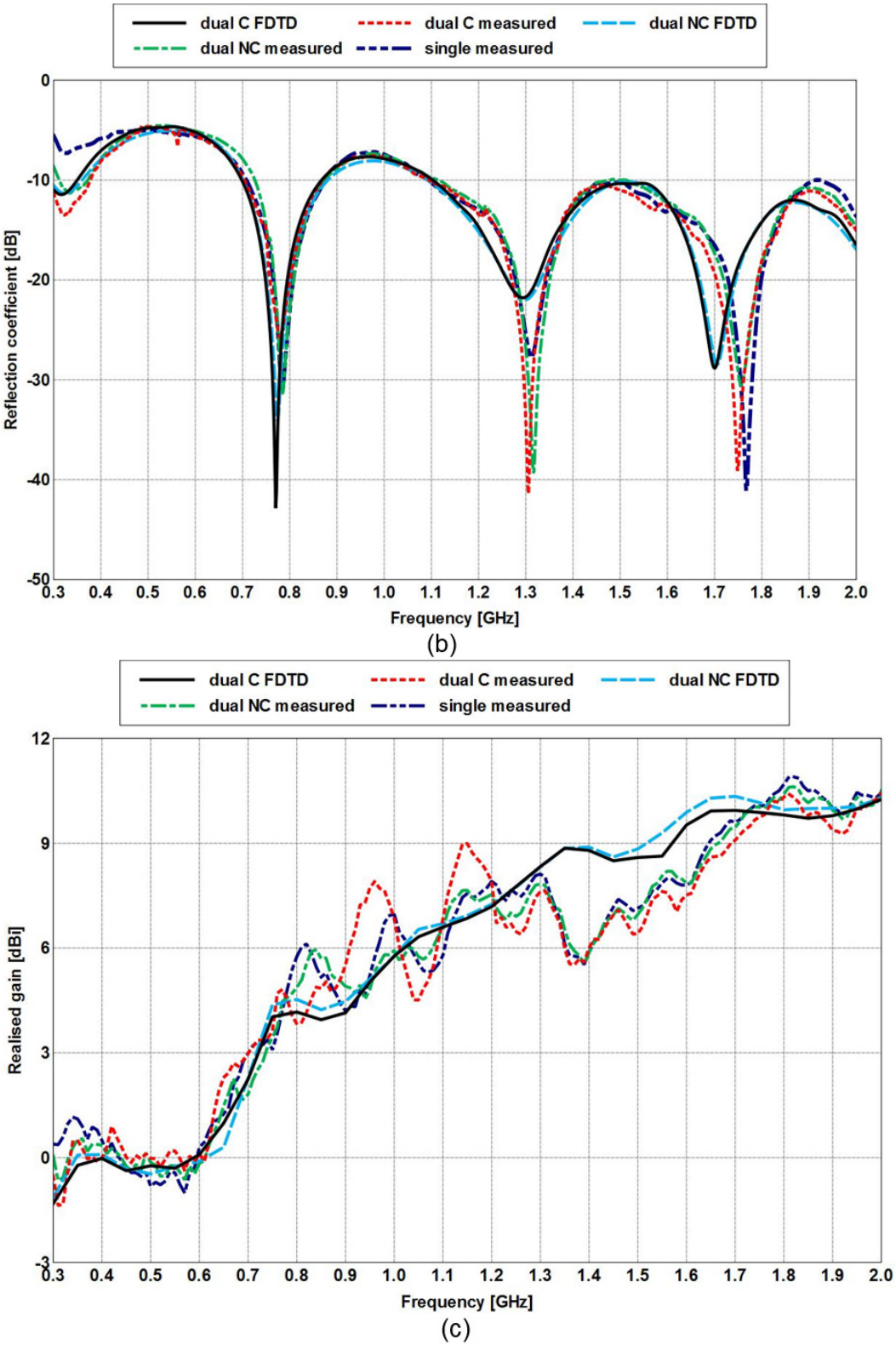

Fig. 24 a) Built corner dual-pol BAV pair, b) simulated and measured reflection coefficient, c) realized gain, d) cross-pol isolation vs. frequency, and e) transient response (continued)

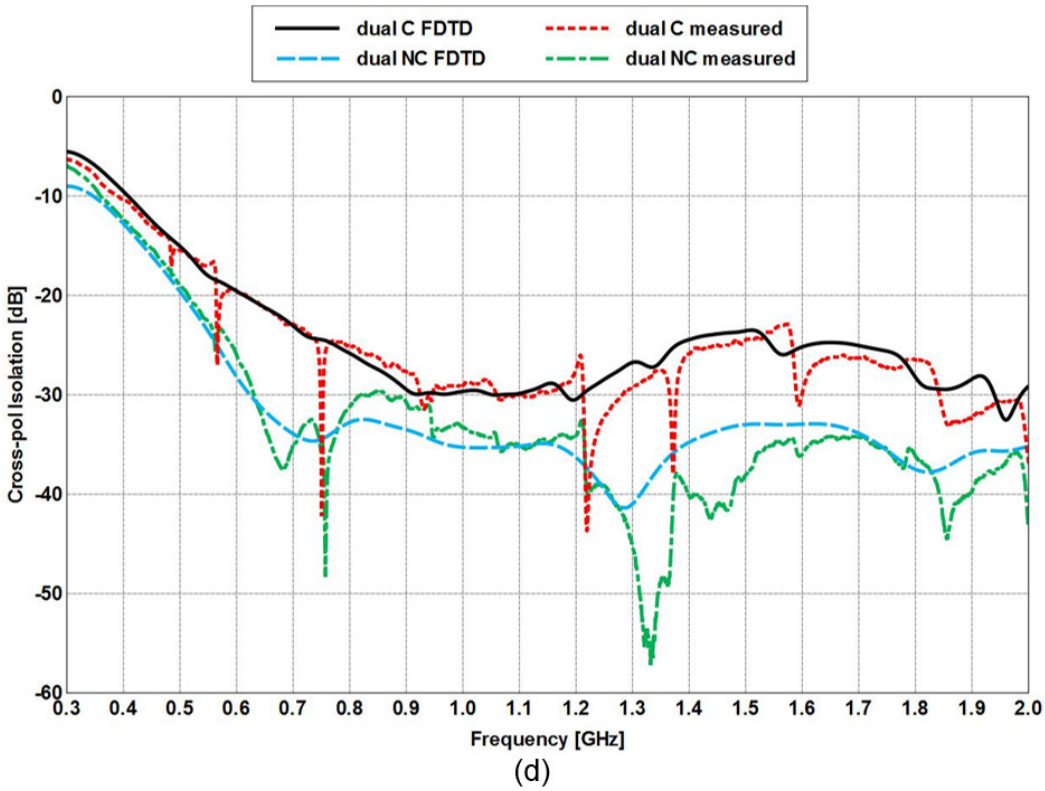

(d)

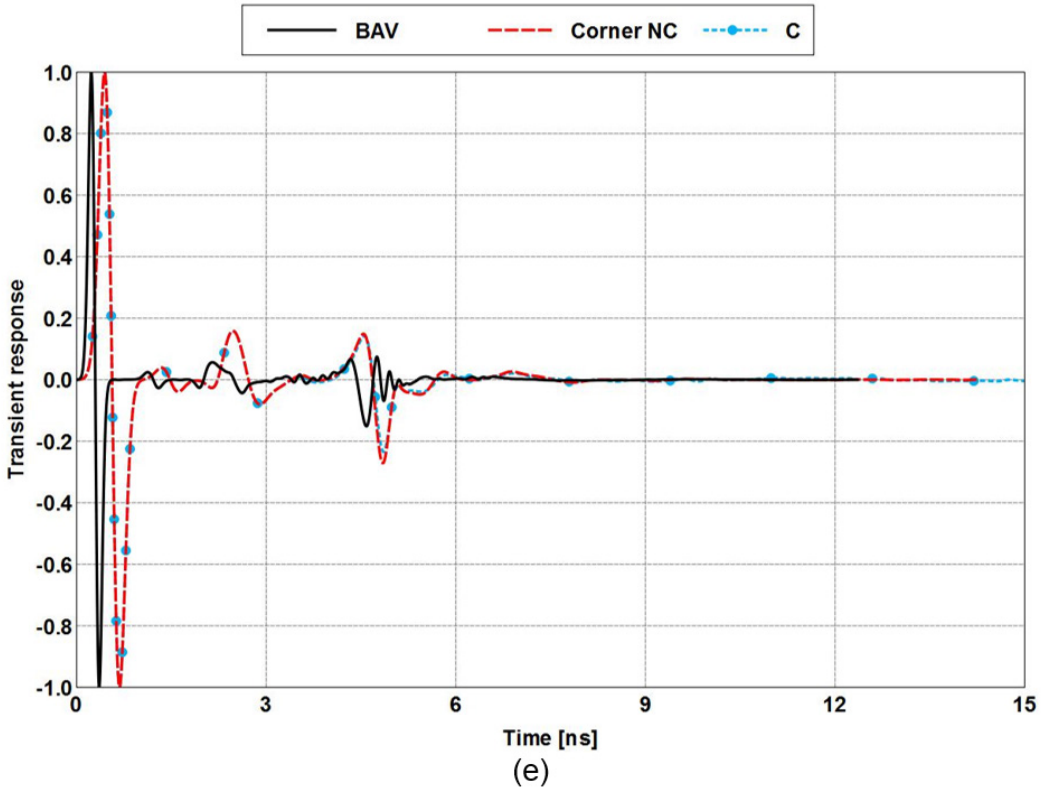

(e)

Fig. 24 a) Built corner dual-pol BAV pair, b) simulated and measured reflection coefficient, c) realized gain, d) cross-pol isolation vs. frequency, and e) transient response (continued)

Measured and simulated radiation patterns at 0.3, 0.7, 1.0, 1.5, and 2.0 GHz are shown in Figs. 25a–c. The E-plane patterns are on the left, and the H-plane on the right. Having 2 elements near each other would, expectedly, influence the radiation pattern, particularly in the side lobes. While connecting the antennas had little effect on the forward gain, it could be argued that connecting them is more detrimental to the side lobe structure than not connecting them. Also, the pair have a larger measured back lobe at 0.7 GHz, which confirms the simulated results of a much smaller F/B between 0.55 and 0.8 GHz. The transient response, Fig. 24e, shows that the neighboring BAV will produce additional ringing in the transient response at a later point in time because of the additional current path to the neighboring BAV termination. Connecting the BAVs produces identical late time ringing.

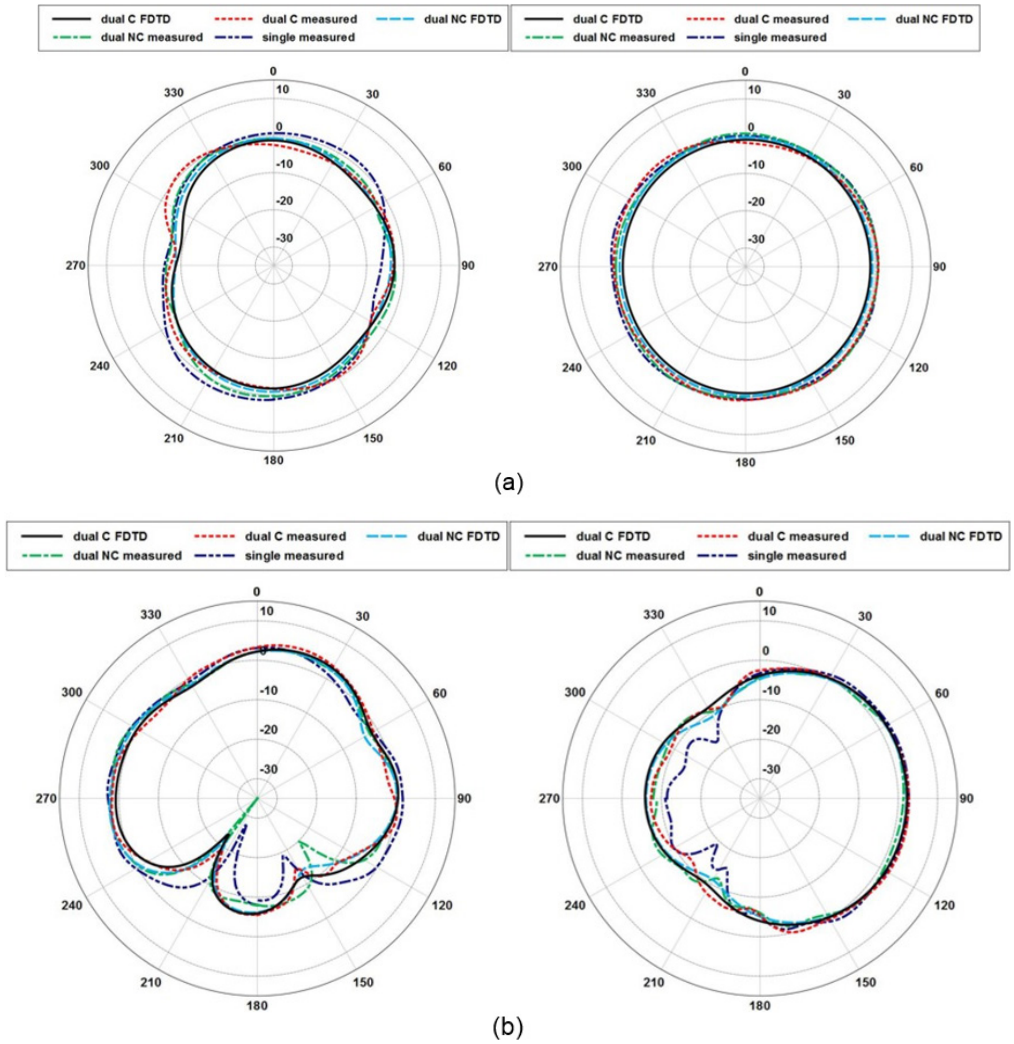

Fig. 25 Simulated and measured radiation patterns for the corner dual-pol BAV with and without a connection at a) 0.3 GHz, b) 0.7 GHz, c) 1.0 GHz, d) 1.5 GHz, and e) 2.0 GHz. E-plane is shown on the left and H-plane is on the right.

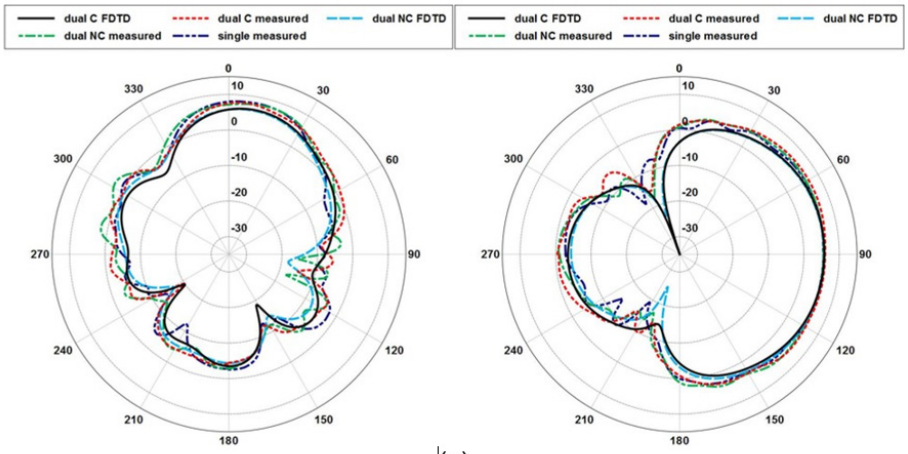

(c)

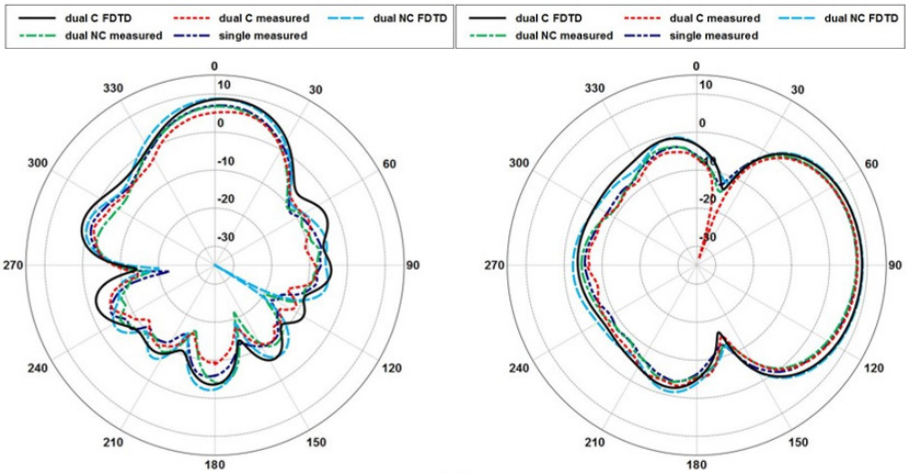

(d)

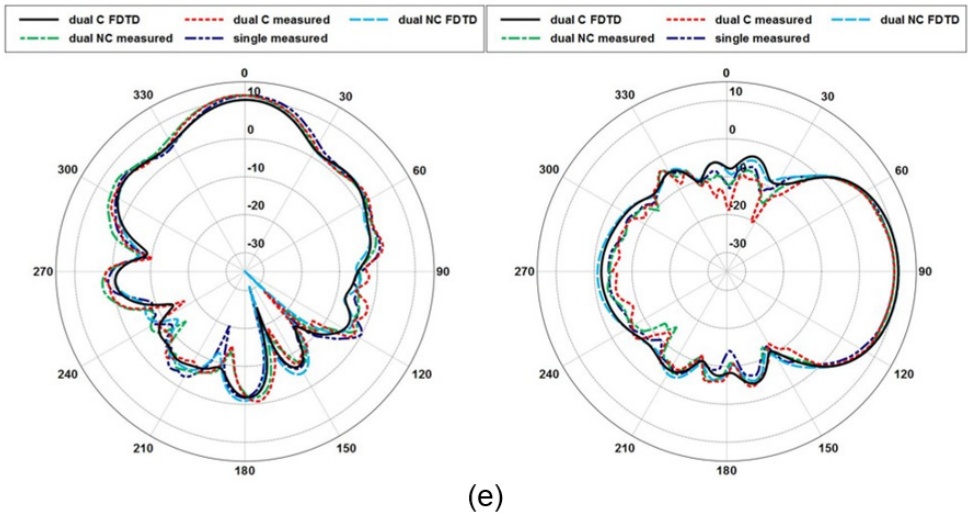

(e)

Fig. 25 Simulated and measured radiation patterns for the corner dual-pol BAV with and without a connection at a) 0.3 GHz, b) 0.7 GHz, c) 1.0 GHz, d) 1.5 GHz, and e) 2.0 GHz. E-plane is shown on the left and H-plane is on the right (continued).

From the study through simulation of the 9 BAV pairs, the corner and side-by-side vertical pairs have the least effect on antenna performance, with the exception of cross-pol isolation. The centered pair—albeit not the preferred arrangement from the viewpoint of individual antenna performance—has the superior low-frequency cross-pol isolation. Between 0.3 and 0.6 GHz, the centered BAV has 30–15 dB of isolation, whereas the corner pair has 6–20 dB of isolation. Low-frequency performance is of critical importance, and with the realized gain being within 1–2 dB of the lone BAV below 1.0 GHz, it could be advantageous to use the centered configuration for all BAVs with neighboring fins matched, Fig. 26, as opposed to mixed pairs, Fig. 17. Doing so would nearly double the width to 4 m. Such an aperture would require further mechanical considerations for construction, as it could be too wide for use in the field.

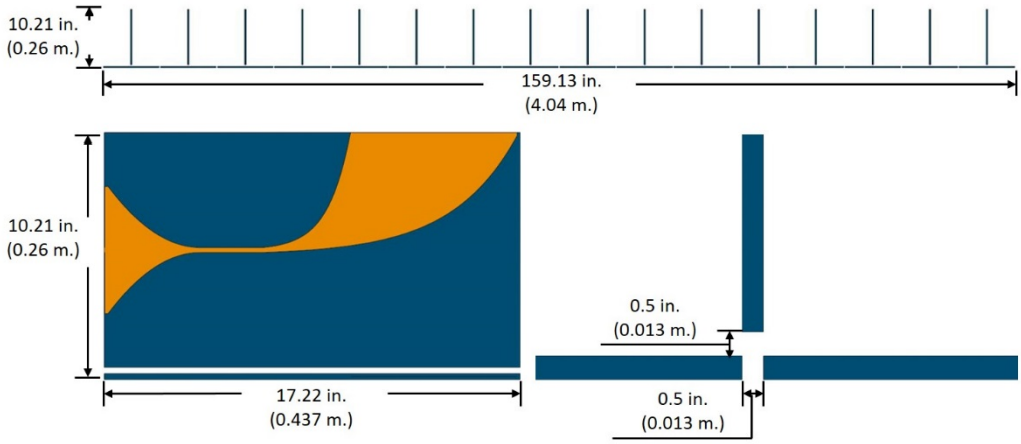

Fig. 26 CAD images and dimensions for aperture with only centered BAV pairs. The bottom row consists of horizontal elements, and the top row is all vertical.

An important point to make as this section closes is the potential cost for producing 32 elements. While the design and analysis for the BAV was done, assuming standard 125-mil-thick Rogers Duroid 5880, the cost for a single board can approach $500 or more. Each BAV would require 2–3 boards and including the cost of tooling hardware and assembly, could cost $1,200–$1,800 to be built in-house. Outsourcing may or may not significantly decrease the unit cost. Switching to a cheaper substrate with similar performance is preferred, but finding such a substrate that also comes in a standard thickness of 125 mil was challenging. The Arlon substrates, sold by Rogers Corp, were the closest in terms of loss and permittivity. The AD350A substrate, $\varepsilon_r = 3.5$ and $\tan\delta = 0.003$, was the closest and would reduce the total cost by a factor of 7.3 at the cost of a 1-dB gain loss above 1.5 GHz due to an 8° and 4° increase in azimuthal and elevation beamwidth, respectively, and a small frequency shift caused by the higher permittivity.

7. Conclusion

This report documents the design by simulation and validation of a balanced antipodal Vivaldi antenna for use as a potential receiving element replacement in US Army Research Laboratory 32-element stepped-frequency ground-penetrating radar within the frequency range of 0.3–2.0 GHz. The initial design process focused on maximizing impedance matching, forward gain, and cross-pol isolation performance. Additional metrics such as half-power beamwidth, F/B, and transient response are compared against the current receiver. The focus of the design was to maximize low-frequency performance, particularly below 1.0 GHz. The current receiver is a Vivaldi type as well but is constructed more akin to a traditional design where the tapered slot is on one side of a single substrate and a stubbed microstrip runs across the gap. Such Vivaldis tend to have –10 dB impedance bandwidths that are limited by the fanned quarter-wave stub on the microstrip; BAV antennas, on the other hand, can have a much broader impedance bandwidth because of the stripline transition and improved cross-pol rejection. However, given the size constraint of this application, neither design will achieve the desired impedance match and bandwidth. Increasing the Vivaldi size can help, but it does not maximize the realized gain below 0.4 GHz and has a poor transient response.

The BAV has 8- to 5-dB larger gain between 0.3 and 0.5 GHz and 2–3 dB above 0.7 GHz. The VSWR is better, though not less than 3.0 across the band, with a max VSWR of 5:1 at 0.3 GHz; the Vivaldi, on the other hand, has a VSWR greater than 10:1 below 0.5 GHz. The transient response is also superior to the Vivaldi with reduced late time ringing. The radiation pattern, as the aperture electrical size increases, is unstable versus frequency. The instability causes frequency variations in the gain and is seen in the E-plane pattern of the BAV but not in the H-plane. The BAV is comparable in length and thickness to the Vivaldi but is about twice as wide. While the built BAV substrate is Rogers Duroid 5880, to reduce unit cost, it is recommended to use the AD350A substrate as the cost is reduced by a factor of 7.3 at the expense of a 1-dB gain loss above 1.5 GHz and a small frequency shift caused by the larger permittivity.

Simulations to predict performance effects of BAV pairs in different arrangements shown in Fig. 18 were documented. It was found that most arrangements had negligible effects on realized gain and impedance match with the exception of the side-by-side horizontal and T-shaped pairs. The horizontal pair showed appreciable effects on performance when opposing fins are next to each other (i.e. grounded fin of one BAV next to the center fin of the other BAV). The T-shaped pair showed that regardless the fin orientation, there was one excitation/termination case for each orientation where the performance was degraded. Overall, the worst effects

produced artifacts in the realized gain of 1 dB (loss or increase) at some frequencies. The cross-pol isolation measurements and simulation showed that although the corner configuration produces the best individual BAV performance, its isolation is in fact worse than the T-shaped below 0.6 GHz. Because cross-pol isolation is critical to the polarimetric array and low-frequency performance was the focus of the design, it is recommended that an aperture configuration like that shown in Fig. 26 be used even though its width is nearly double the 2.2-m requirement.

8. References

1. Balanis CA. Advanced engineering electromagnetics. 2nd ed. Hoboken (NJ): John Wiley and Sons; 2012. p. 143.
2. Stutzman WL, Thiele GA. Antenna theory and design. 3rd ed. Edison (NJ): John Wiley and Sons; 2013. p. 488–498.
3. FEKO. Stellenbosch (South Africa): Altair Engineering Inc.; 2017 [accessed 2017 Apr 7]. www.feko.info.
4. GEMS. Fairfax (VA): 2COMU; 2009 [accessed 2017 July 7]. www.2comu.com.
5. Smith GD, Harris RW, Ressler MA, Stanton B. Wideband Vivaldi notch antenna design for UWB SIRE VH/UHF/Radar. Adelphi (MD): Army Research Laboratory (US); 2008 March. Report No.: ARL-TR-4409.
6. Coburn WO, McCormick SA. Antenna array development for the radio frequency enabled detection, location, and improvised explosive device (IED) neutralization evaluation (REDLINE) system. Adelphi (MD): Army Research Laboratory (US); 2016 July. Report No.: ARL-TR-7712.
7. McCormick SA, Zaghloul AI, Harrison AC. A rugged ultra-wideband (UWB) circular planar monopole for multichannel radar. Adelphi (MD): Army Research Laboratory (US); 2016 March. Report No.: ARL-TR-7630.
8. Guillanton E, Dauvignac JY, Pichot C, Cashman J. A new design tapered slot antenna for ultra-wideband applications. Microwave and Optical Technology Letters. 1998;(19)4:286–289.
9. Gazit E. Improved design of the Vivaldi antenna. IEEE Proceedings. 1988;(135)2:89–92.
10. Langley JDS, Hall PS, Newham P. Novel ultrawide-bandwidth Vivaldi antenna with low crosspolarisation. Electronics Letters. 1993;(29)23:2004–2005.
11. Schaubert DH. Wide-band phased arrays of Vivaldi notch antennas. 10th International Conference on Antennas and Propagation. 1997;(436):1.6–1.12.

Appendix A. Effects of a Wide Stripline Ground, Substrate Thickness, and Lens on Reflection Coefficient and Realized Gain

This Appendix documents the simulated results for the effects of a wider stripline ground, thicker substrate, and an imbedded shaped dielectric lens on balanced antipodal Vivaldi (BAV) performance. Figures A-1a and A-1b show the simulated reflection coefficient for the BAV shown in Fig. 8 of the main text with a wider ground. The ground for the BAV is the flared fins near the feed (i.e., grounded strips for the stripline). Two cases were simulated: one with the ground as built and one with the width the same as the substrate width. Widening the ground exponential taper till it is the same width as the substrate improves the impedance match across the band, including the low frequencies, as seen in Fig. A-1a. However, this improved match does not necessarily translate to an improved forward realized gain, Fig. A-1b. With the exception of frequencies near 0.5 GHz where the gain is about 2 dB larger, the gain sees practically no improvement, and it is nearly 2 dB less at 0.7 GHz where the pattern splits. The focus of the design was to improve the low-frequency performance, in particular the realized gain, as it takes into consideration the impedance match. Because the wider ground produced reduced gain at some frequencies, it was not included in the final design.

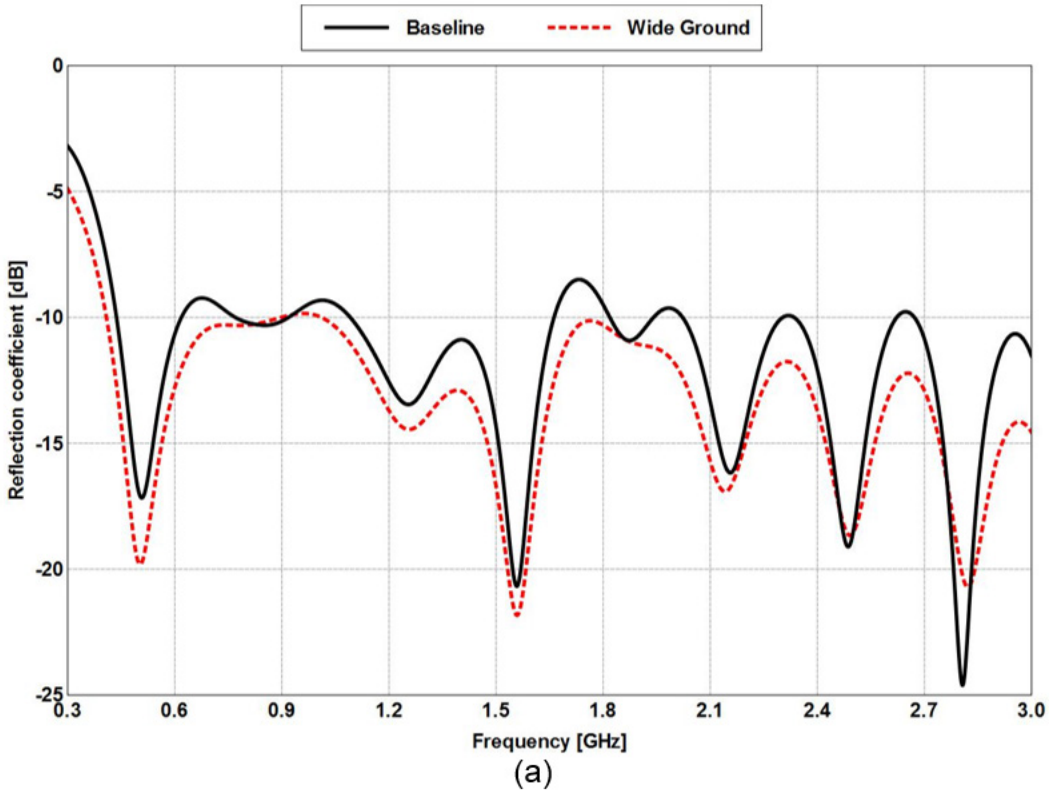

Fig. A-1 Simulated a) reflection coefficient and b) forward realized gain vs. frequency of the BAV with and without a wider stripline ground

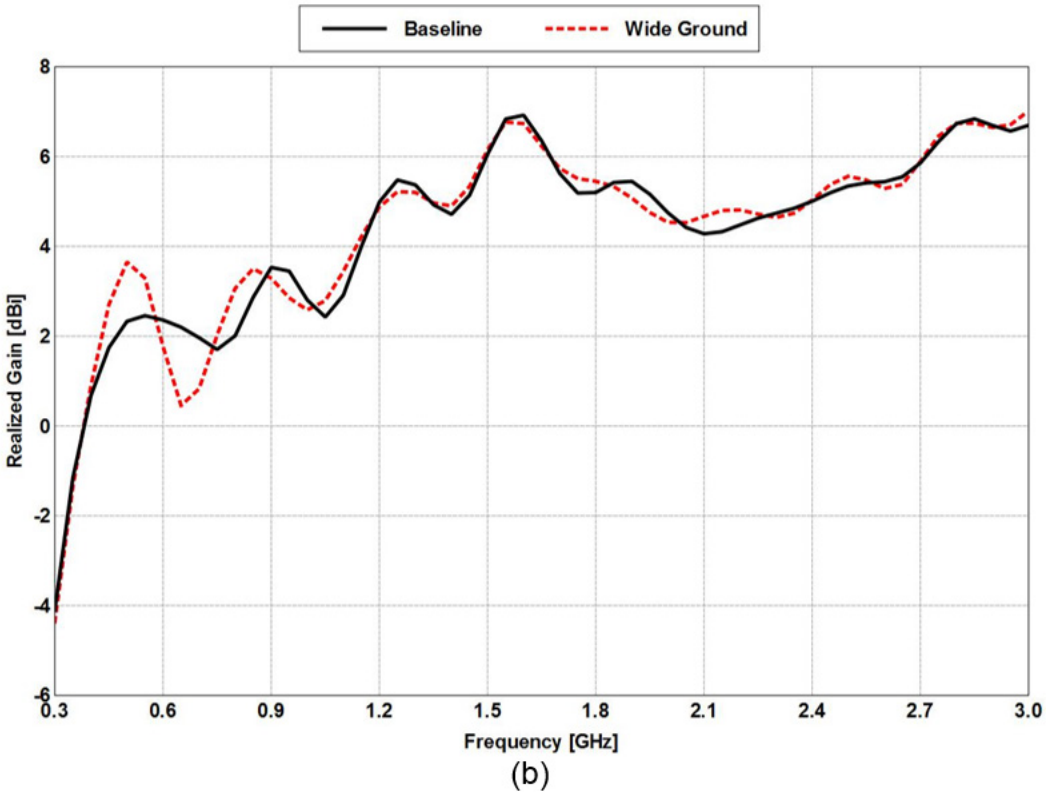

Fig. A-1 Simulated a) reflection coefficient and b) forward realized gain vs. frequency of the BAV with and without a wider stripline ground (continued)

Figures A-2a and A-2b show the simulated reflection coefficient and realized gain versus frequency of the BAV shown in Fig. 8 for varying substrate thickness; the stripline width is adjusted for the change in thickness to maintain the same input impedance. Substrate thicknesses of 60, 180, 300, 420, and 480 mils were considered. As expected, increasing the substrate thickness can help to improve the impedance match up to a point, Fig. A-2a. From the shown results, the substrate thickness for the best impedance match would be around 420 mils as it gives the lowest frequency match while maintaining a near –10-dB reflection coefficient up to 3.0 GHz and beyond. The realized gain results, Fig. A-2b, show the expected behavior of worsening gain for too thick a substrate owing to surface waves. Where the 420 mils thickness is best for the impedance match, the 180 mils thickness would be the best for the realized gain as it has the flattest gain behavior vs. frequency. Just like with the impedance match, if the substrate is too thick or too thin the gain is not optimal. Considering both the impedance match and the forward realized gain, 300 mils would be the preferred substrate thickness.

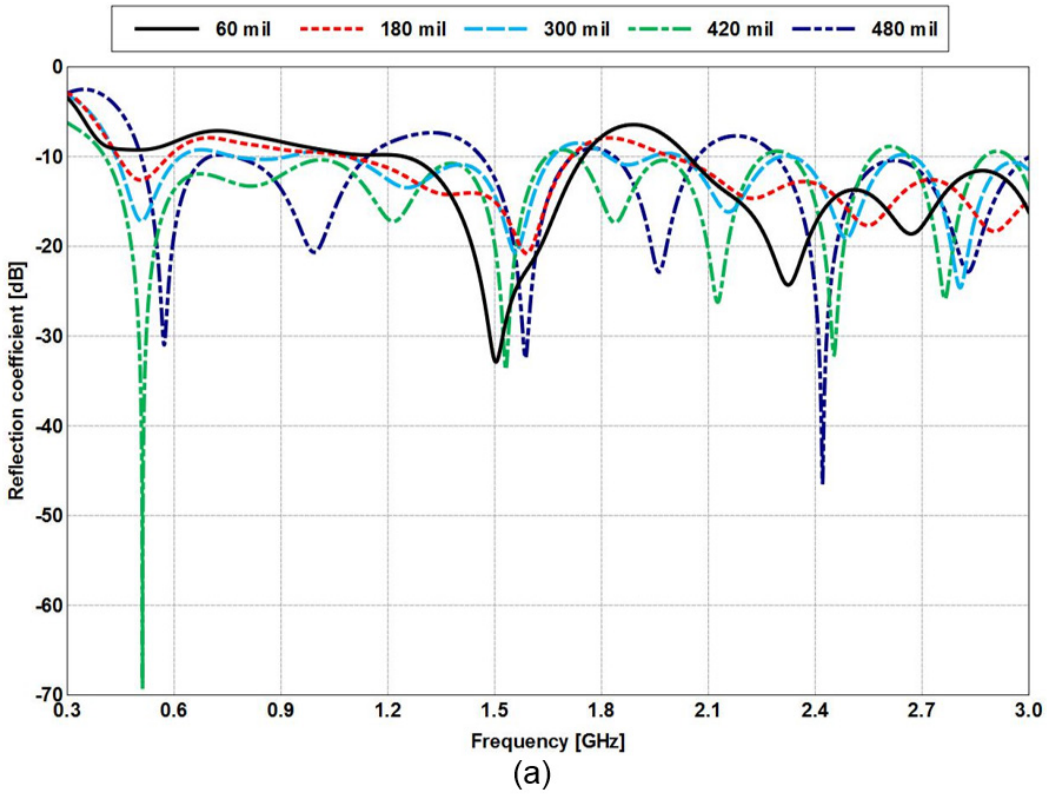

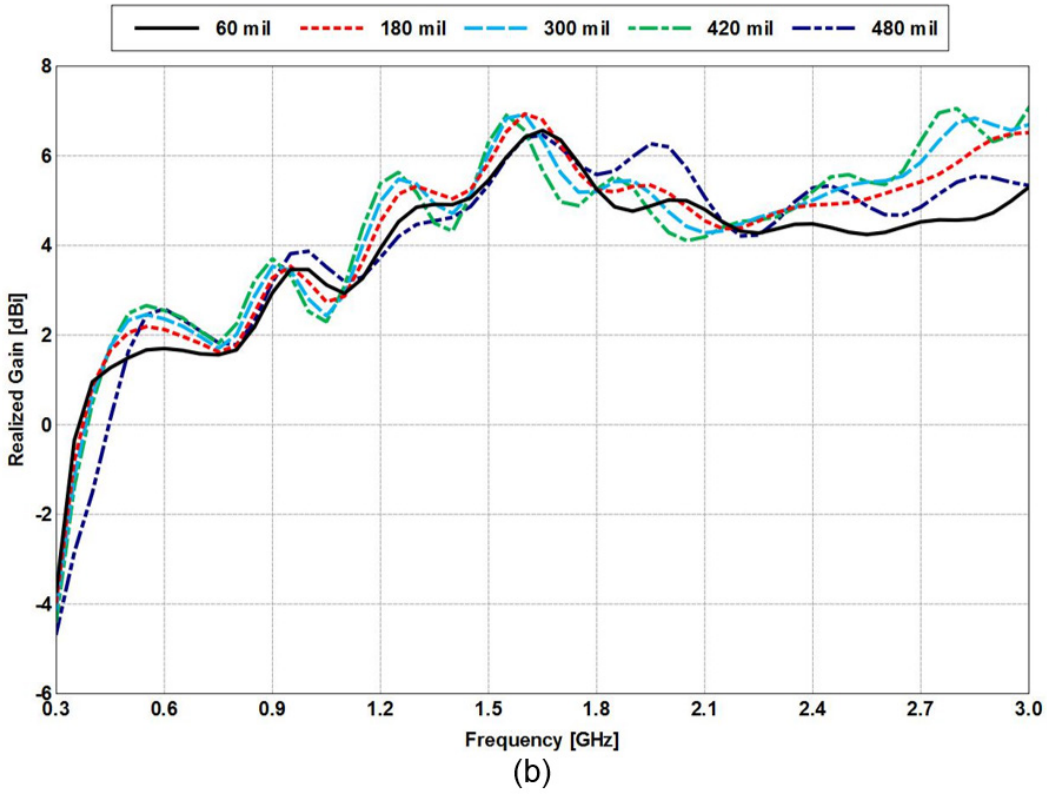

Fig. A-2 Simulated a) reflection coefficient and b) forward realized gain vs. frequency of the BAV for different substrate thicknesses

Figure A-3a shows the computer-aided design (CAD) BAV model with an embedded shaped dielectric lens. The lens permittivity is 6.0 and is lossless. The shape was taken from the literature and was not modified to achieve the best performance possible.[1] The permittivity was chosen to conform to what can be found readily available from commercial printed circuit board substrate manufactures. The lens is the same thickness as the BAV and extends about 1.5 inches past the BAV edge. The purpose of the shaped lens is to produce a uniform (or near uniform) phase front radiating from the tapered slot region by introducing a spatially varying phase delay. The varying phase delay is achieved by shaping the lens such that fields nearer the center of the tapered slot are delayed the most compared to those fields farthest away from the slot (i.e., all radiating paths are equal).[2] The embedded lens functions similar to a director in that it concentrates the aperture field within the slot.

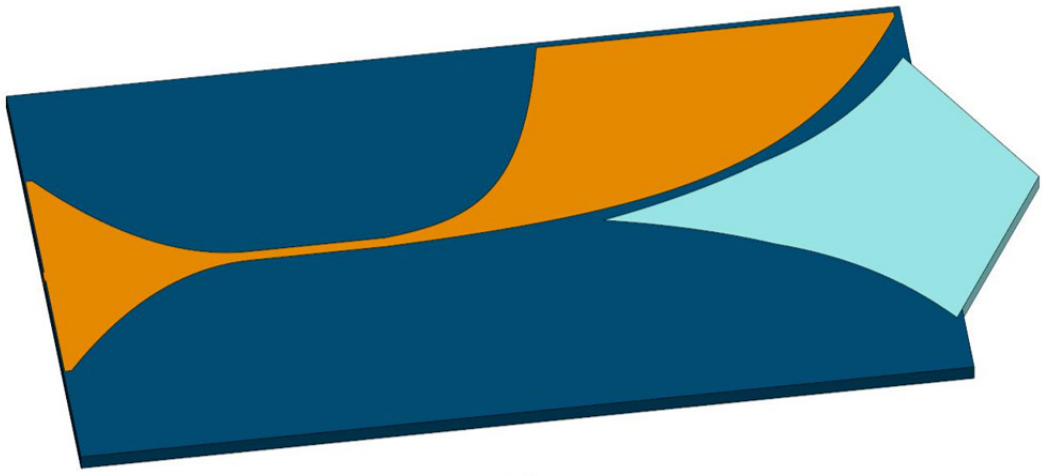

(a)

Fig. A-3 a) BAV with embedded shaped dielectric lens, b) simulated reflection coefficient, and c) realized gain vs. frequency with and without the lens

[1] Bourqui J, Okoniewski M, Fear EC. Balanced antipodal Vivaldi antenna with dielectric director for near-field microwave imaging. IEEE Transactions on Antennas and Propagation. 2010;(58)7:2318–2326.

[2] Volakis JL. Antenna engineering handbook. 4th ed. New York (NY): McGraw-Hill; 2007. p. 18–2.

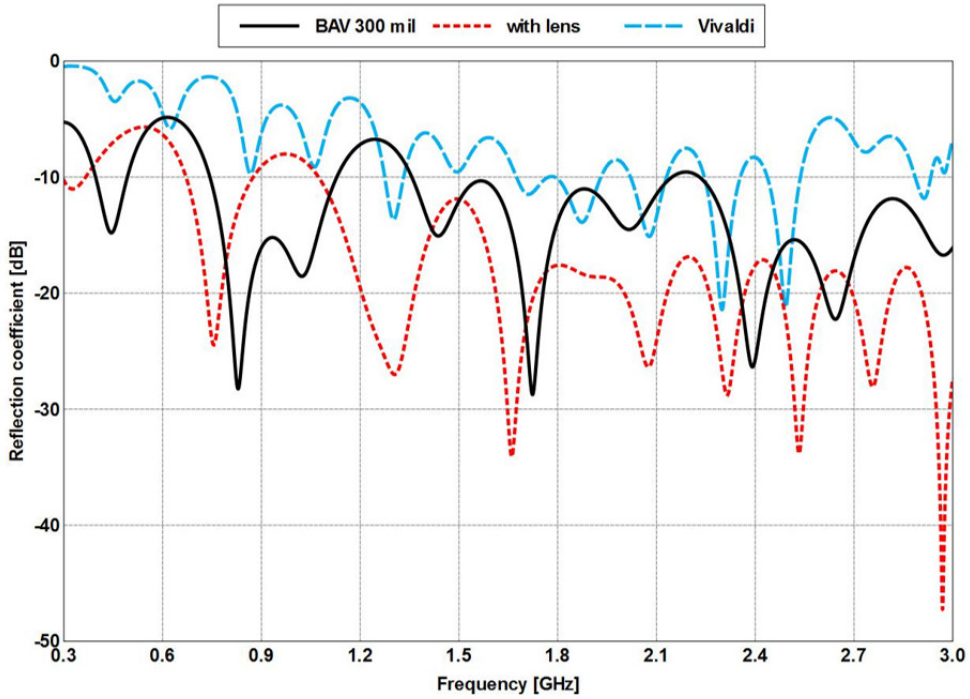

(b)

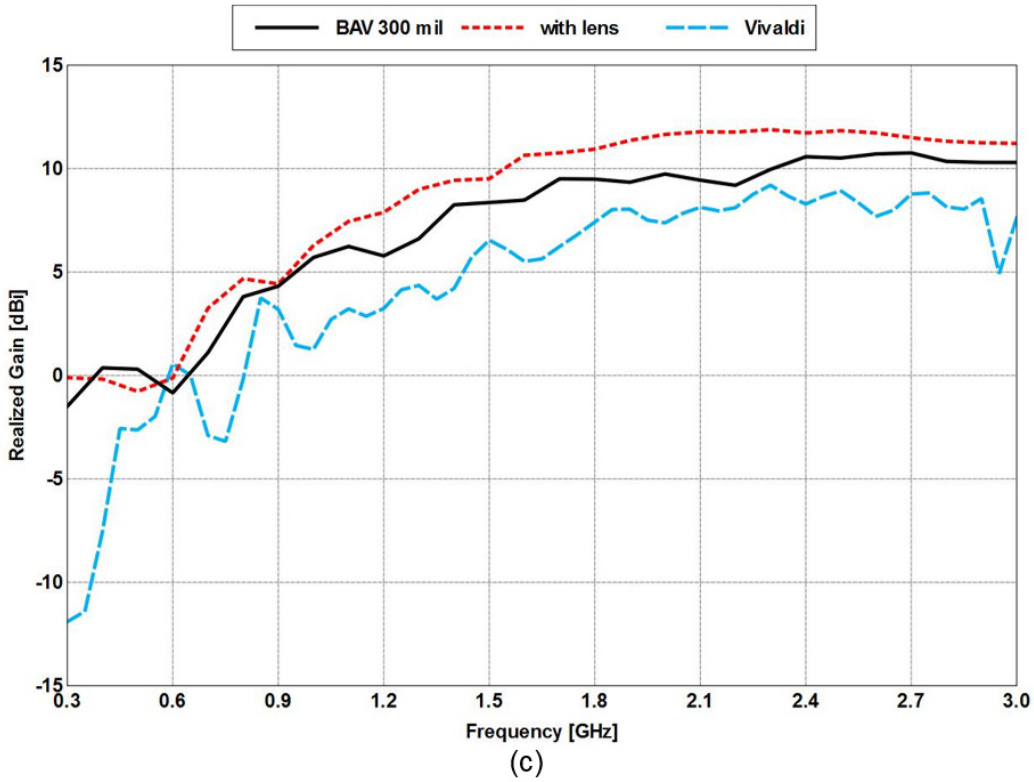

(c)

Fig. A-3 a) BAV with embedded shaped dielectric lens, b) simulated reflection coefficient, and c) realized gain vs. frequency with and without the lens (continued)

Embedded dielectric lenses are most commonly seen in waveguides and horns, which also serve as a means to reduce the size of the aperture. If successful, the embedded lens should give modest improvements in realized gain as well as added benefits of material loading, such as reduced electrical size. For the BAV, the embedded lens achieves both in addition to an improved impedance match as seen in Fig. A-3b and A-3c. The cause of the improved impedance match was not explored, but a hypothesis would be that a reduction in the wave impedance (i.e., improved impedance match to free space) has been achieved and so there is a better transmission of fields out of the substrate away from the feed and into free space. The lens improves the gain across the frequency band with modest 1-dB increases at frequencies below 1.0 GHz, to a more appreciable improvement of 2 dB at frequencies above 1.0 GHz. The unwanted side effect of a thicker, higher permittivity medium on gain can be seen above 3.0 GHz where there is a 1- to 2-dB reduction; this could, however, be due to the lens not extending far enough into the tapered slot to work for those higher frequencies.

INTENTIONALLY LEFT BLANK.

Appendix B. Balanced Antipodal Vivaldi (BAV) Schematic

This Appendix presents a BAV schematic (Fig. B-1). Specifications for the cutout and connector are given in Section 4 of the main text.

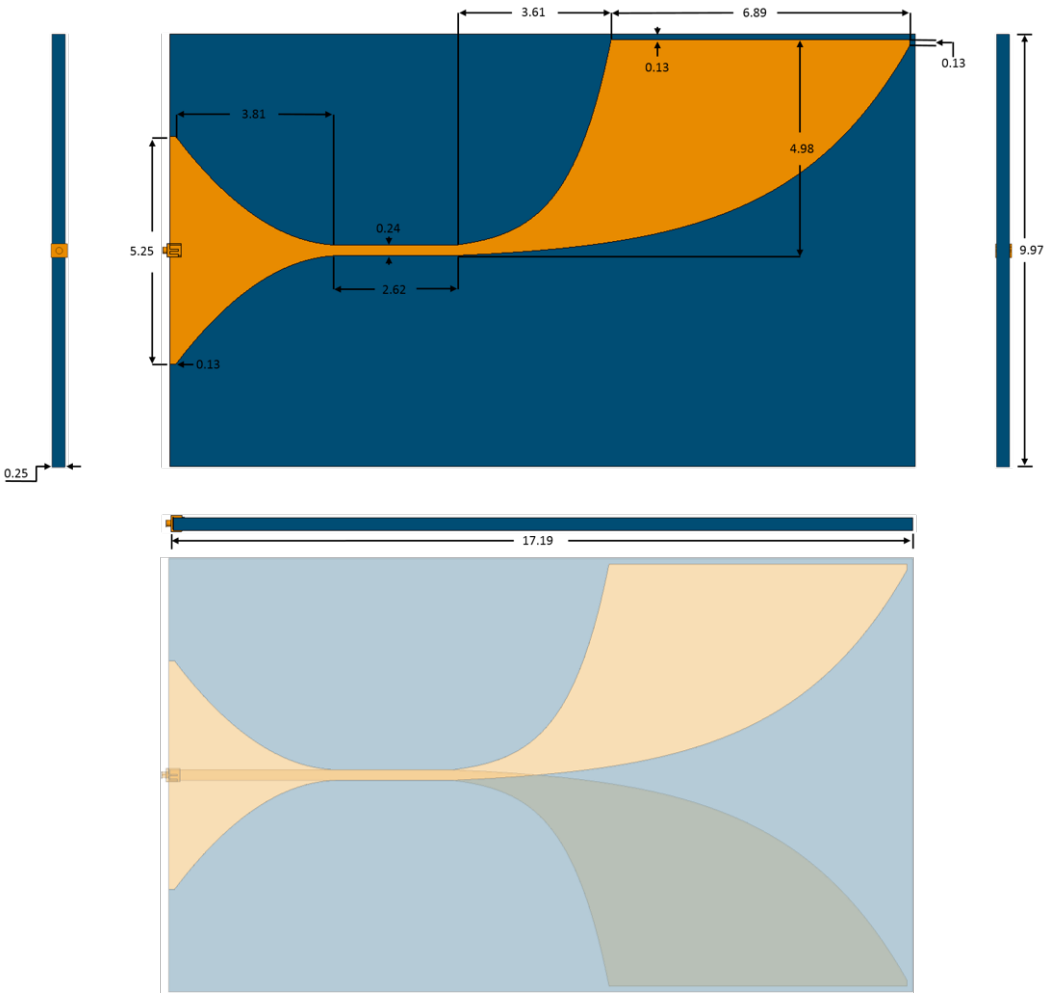

Fig. B-1 BAV schematic and partially transparent top view. Units are in inches.

List of Symbols, Abbreviations, and Acronyms

BAV	balanced antipodal Vivaldi
CAD	computer-aided design
cross-pol	cross polarization
F/B	front-to-back ratio
FLGPR	forward-looking ground-penetrating radar
GEMS	General Electromagnetic Solver
LPDA	logarithmic periodic dipole array
MoM	Method of Moments
PEC	perfectly electrically conducting
UWB	ultra-wideband
VSWR	voltage standing wave ratio

1 (PDF) DEFENSE TECHNICAL INFORMATION CTR DTIC OCA

2 (PDF) DIR ARL
RDRL DCM
IMAL HRA RECORDS MGMT
RDRL DCL
TECH LIB

1 (PDF) GOVT PRINTG OFC
A MALHOTRA

4 (PDF) DIR USARL
RDRL SER M
S A MCCORMICK
W O COBURN
RDRL SER U
B R PHELAN
K D SHERBONDY